AFRPL-TR-74-52

ANALYTICAL RELATIONSHIPS FOR ESTIMATING THE EFFECTS OF X-RAYS ON MATERIALS

SPECIAL REPORT

MCDONNELL DOUGLAS ASTRONAUTICS COMPANY, WEST
5301 BOLSA AVENUE
HUNTINGTON BEACH, CALIFORNIA 92647

AUTHOR: R. W. LANGLEY

SEPTEMBER 1974

APPROVED FOR PUBLIC RELEASE
DISTRIBUTION UNLIMITED

AIR FORCE ROCKET PROPULSION LABORATORY
DIRECTOR OF SCIENCE AND TECHNOLOGY
AIR FORCE SYSTEMS COMMAND
EDWARDS, CALIFORNIA 93523

FOREWORD

The work described in this report was conducted by the McDonnell Douglas Astronautics Company under Independent Research and Development Account No. 81205-202. It is published as an Air Force technical document because the material represents the analytical framework that is a central part of the "Rocket Propulsion System Hardening Design Handbook, Volume 1, Nuclear" developed by McDonnell Douglas Astronautics Company for the Air Force Rocket Propulsion Laboratory, under Contract No. F04611-73-C-0042.

This report was prepared under Purchase Order No. F04700-75-M-2114. The Air Force Project Officer was Mr. G. Allen Beale.

This test report has been reviewed and approved.

FOR THE COMMANDER

PAUL J. DAILY,
Colonel, USAF
Chief, Technology Division

UNCLASSIFIED

SECURITY CLASSIFICATION OF THIS PAGE *(When Data Entered)*

REPORT DOCUMENTATION PAGE		READ INSTRUCTIONS BEFORE COMPLETING FORM
1. REPORT NUMBER AFRPL TR-74-52	2. GOVT ACCESSION NO.	3. RECIPIENT'S CATALOG NUMBER
4. TITLE *(and Subtitle)* ANALYTICAL RELATIONSHIPS FOR ESTIMATING THE EFFECTS OF X-RAYS ON MATERIALS		5. TYPE OF REPORT & PERIOD COVERED Special Report 6. PERFORMING ORG. REPORT NUMBER
7. AUTHOR(s) R. W. Langley		8. CONTRACT OR GRANT NUMBER(s)
9. PERFORMING ORGANIZATION NAME AND ADDRESS McDonnell Douglas Astronautics Company, West 5301 Bolsa Avenue Huntington Beach, California 92647		10. PROGRAM ELEMENT, PROJECT, TASK AREA & WORK UNIT NUMBERS
11. CONTROLLING OFFICE NAME AND ADDRESS Air Force Rocket Propulsion Laboratory Director of Science and Technology Air Force Systems Command Edwards, California 93523		12. REPORT DATE September 1974 13. NUMBER OF PAGES 98
14. MONITORING AGENCY NAME & ADDRESS*(if different from Controlling Office)*		15. SECURITY CLASS. *(of this report)* UNCLASSIFIED 15a. DECLASSIFICATION/DOWNGRADING SCHEDULE N/A

16. DISTRIBUTION STATEMENT *(of this Report)*

APPROVED FOR PUBLIC RELEASE; DISTRIBUTION UNLIMITED

17. DISTRIBUTION STATEMENT *(of the abstract entered in Block 20, if different from Report)*

18. SUPPLEMENTARY NOTES

19. KEY WORDS *(Continue on reverse side if necessary and identify by block number)*

x-ray effects
material response
analytical relationships
design equations

20. ABSTRACT *(Continue on reverse side if necessary and identify by block number)*

This report contains a summary of analytical relationships that have been derived for estimating the effects of x-rays on materials. The relationships are generally applicable to any system. Optimum conditions for any range of radiation spectra are emphasized; however, specific spectra are also treated. The relationships are especially useful because of their convenience and generality, and their accuracy is comparable to that of

DD FORM 1 JAN 73 1473 EDITION OF 1 NOV 65 IS OBSOLETE

UNCLASSIFIED

SECURITY CLASSIFICATION OF THIS PAGE *(When Data Entered)*

20. ABSTRACT (Continued)

specialized computer calculations. Input data on empirical material properties and damage criteria remain the greatest source of uncertainty, rather than analytical modeling approximations.

CONTENTS

UNIT CONVERSION RELATIONS

1 g/cm^3 (units of weight density) = 1 dyne-sec^2/cm^4 (units of mass density)

1 gram = 1 dyne-sec^2/cm (= 980.7 dynes at acceleration of 1 gravity)

1 dyne = 1 gram - cm/sec^2

1 erg = 1 dyne - cm = 10^{-7} joules

1 calorie = 4.186×10^7 ergs = 4.186×10^{-5} megabar-cm^3

1 tap = 1 dyne-sec/cm^2 = 1 bar-μsec

1 bar = 10^6 dynes/cm^2 = 14.5 psi = 0.987 atmosphere

1 psi = 69,000 dynes/cm^2 = 0.69×10^{-7} megabar = 70.31 g/cm^2

1 kilobar = 10^3 bars = 10^9 dynes/cm^2

1 megabar = 10^3 kilobars = 10^{12} dynes/cm^2

1 cal/g°C = 1 Btu/lb°F

1 ft/sec = 30.48 cm/sec = 30.48×10^{-6} cm/μsec

1 kev = 10^3 electron volts = 1.603×10^{-9} ergs

Section 1
INTRODUCTION AND SUMMARY

This report summarizes analytical relationships derived for estimating the effects of x-rays on materials. Since all major x-ray effects are treated in a general way, they are generally applicable to anything exposed to x-rays. Although the relationships were developed primarily for the designer and systems analyst, their quality is comparable to computer codes so they are also useful to the technologist.

The effects covered include energy deposition in single and multiple materials, front-face mass removal, structural heating, blowoff impulse, stress generation by impulse loads and thermal loads, stress wave attenuation in undistended and distended materials, and structural response. Optimum energy spectra which maximize an effect for a given fluence are emphasized; however, specific spectra are also treated.

Except for stress wave attenuation in distended materials, the relationships and their demonstrated general validity for effects analysis are new—they were developed during the past year. The motivation for developing an analytical approach was to circumvent the difficulties associated with : (1) the need to provide practical understanding of individual and combined x-ray effects to individuals not conversant with x-ray effects, (2) the numerous factors involved in analyzing x-ray effects, (3) the vast number of materials and material combinations associated with some systems, (4) the determination of spectrally optimized effects, (5) the need for flexibility in accommodating refinements in damage or failure criteria, (6) the tedium and crudeness of existing analytical techniques, (7) the designer's lack of convenient access to computerized analytical techniques, and (8) the inherent problems of over-dependence on computerized numerical analysis.

The resulting generalized analytical relationships are simple closed-form equations. With only three exceptions, they are all derived from basic theoretical concepts rather than empirical correlations; otherwise, the task would have been impractical. They have been compared with computer analyses performed with energy-deposition codes and hydrodynamic codes, and the comparisons have shown the equations to produce, over the complete practical ranges of parameters, the results of the computer codes to within generally 10 to 30 percent. It is not clear how much of this difference is due to approximations in the equations and how much is due to errors in the codes. In some cases, the error appears to be in the codes, for example, in consistent discontinuities in computer results which have no physical basis, and the error becomes apparent only when a parametric correlation is attempted. When the differences between calculations that involve a number of parameters are small, it takes considerable time and effort to determine the exact sources of the differences. There have been a few isolated cases when the difference between analytical results and computer results has been as much as a factor of 2 (e.g., the empirical energy deposition relationships); however, for the same or similar cases, two computer programs gave results that differed by greater than a factor of 2, presumably because they use different sets of x-ray mass absorption coefficients.

In adopting a perspective for the accuracy of any analytical tool for vulnerability analysis, it is helpful to realize that, from a practical standpoint, useful precision is limited by the accuracy of materials data, failure criteria, and the reality of assumptions regarding radiation environments. The uncertainties of all of these far exceed the uncertainty in the present analytical modeling approximations.

A large number of comparisons have been made. However, because of the numerous relationships and ranges of parameters involved, it has not been practical to make a comprehensive study of the accuracy of the analytical relationships. It has been necessary to present the results of the comparisons that have been made in somewhat general terms; documentation has not been possible due to the limited scope of effort. Nevertheless,

sufficient comparisons have been made over the full ranges of parameters of the individual relationships that their validity and nominal accuracy have been established.

The objective has been to duplicate computer analyses as closely as possible. Aside from the benefits of an uncomplicated analysis, such an approach gives numerical results which have the same state-of-the-art limitations relating to material properties, failure criteria, and theoretical constructs as the computer programs it seeks to emulate. These same limitations on the application of theoretical tools make them indispensable to a rational design approach because of the even more severe restrictions they impose on the alternate approach of empiricism[1].

In addition to presenting the derivation of equations for each phenomenon, the last section of the report combines these equations to obtain explicit expressions for fluence thresholds for various failure mechanisms and situations relevant to propulsion systems. Others can be similarly derived.

An attempt has been made to maintain consistent units and symbols throughout. They are defined in each context. Units of calories, grams, centimeters, microseconds, kilobars, and kilotaps have been used consistently. A set of unit conversion relations has been included for reference.

---

[1] J. Watcher, Rocket Propulsion System Hardening Design Handbook. McDonnell Douglas Paper WD 2353. Presented at the Fourth Symposium on Nuclear Survivability of Propulsion and Ordnance Systems, Defense Nuclear Agency Report, 1974.

Section 2

X-RAY ENERGY DEPOSITION

The most fundamental quantity required for x-ray effects analysis is the x-ray energy deposition in a given material or laminate; the analysis of all effects relies upon this information. An x-ray spectrum is, for convenience, often characterized by a single blackbody temperature expressed in kev (10^3 electron volts). An x-ray environment can also be characterized by a range of blackbody temperatures. The objective of this section is to derive useful analytic relationships for energy deposition for blackbody energy spectra.

2.1 MAXIMUM DOSE FOR A RANGE OF BLACKBODY SPECTRA

2.1.1 Single Material

For a range of blackbody temperatures and for a given point within a material, a unique quantity is the maximum dose (i.e., energy depostion) for a given fluence. The exact expression for the dose in a single material is

$$D(x, Z, T) = \phi \int_0^\infty B(E, T) \exp\left[-\mu(Z, E)\rho x\right] \mu(Z, E)\, dE \qquad (1)$$

where D is the dose in cal/g, x is the thickness variable in cm, Z is the atomic number of the material, T is the blackbody temperature in kev, ϕ is the incident x-ray fluence in cal/cm^2, ρ is the material density in g/cm^3, $\mu(Z, E)$ is the x-ray mass absorption coefficient in cm^2/g, E is the x-ray (photon) energy in kev, and B(E, T) is the blackbody function given by

$$B(E, T)dE = \frac{15}{\pi^4}\left(\frac{y^3}{e^y - 1}\right)dy \qquad (2)$$

where $y = E/T$. The integral of Equation (2) from zero to infinity is one.

Disregarding absorption edges, it is well known that a good approximation for the mass absorption coefficient is

$$\mu(Z, E) = \mu_1 Z^n E^{-m} \tag{3}$$

where μ_1 is the reference value at 1 kev. For the range of energies of practical interest, $n \approx m \approx 3$.

Defining the variable $\psi = \mu_1 Z^n E^{-m} \rho x$, Equation (1) becomes

$$D = \frac{15}{m \pi^4} \left(\frac{\phi}{\rho x}\right) \int_0^\infty \left(\frac{y^4}{e^y - 1}\right) e^{-\psi} \, d\psi \tag{4}$$

The objective is to maximize D by maximizing the integral. Since $e^{-\psi} d\psi$ varies far more strongly with y than does the blackbody function in parentheses, a good assumption is to remove the blackbody function from the integral and maximize it, with the remainder of the integral becoming unity. Thus,

$$\text{Max} \left(\frac{y^4}{e^y - 1}\right) \approx \text{Max} \, (y^4 e^{-y}) = 4^4 e^{-4} \tag{5}$$

Substituting this and m = 3 into Equation (4) gives for the maximum dose for any fluence, in any material,

$$D_m = \left[\frac{15 \, (4)^4 \, e^{-4}}{3\pi^4}\right] \frac{\phi}{\rho x} = 0.24 \, \frac{\phi}{\rho x} \tag{6}$$

Because this is an optimum, the variation of dose with all parameters is weakest near D_m. Also, the floating parameter which is optimized (i.e., y) has the effect of obscuring the absorption edges in higher-atomic-number materials so that they are manifested only in terms of an average m, a

parameter that is a weak function of Z and a weaker function of E. This is verified by parametric computer calculations with a typical one-dimensional point-kernel (exponential attenuation) x-ray transport code using the mass absorption coefficients of Marotta.[2]

Table 1 lists coefficients of Equation (6) that were determined by parametric computer calculations. The coefficients naturally fall into three categories: Group 1, $Z \leq 6$; Group 2, $12 \leq Z \leq 30$; and Group 3, $Z \geq 40$. However, the single coefficient of 0.24 is within ±20 percent for all materials, and is sufficiently accurate for virtually all situations which do not fall outside a specified range of T. (What to do when they do fall outside is discussed in Section 2.2). Equation (6) is therefore applicable to any homogeneous material, and is independent of all physical properties except density. Greater accuracy is obtained by using the coefficients of Table 1, but it is helpful to realize that since blackbody spectra or any other idealized spectra represent convenience more than reality, consistency is more important than absolute accuracy once a practically acceptable level of accuracy is attained.

The variation of the mass absorption coefficient is shown in Figure 1 for carbon, aluminum, iron, and tungsten. The sharp discontinuities caused by the various orbital-electron shells (designated K, L, M, etc.) are, in effect, completely smoothed out by optimizing D in terms of a dispersive spectrum. For energies higher than the K-shell potential, $m = 3.0$ for all elements, and for all lower energies, $m = 2.5$. Between carbon and aluminum, $n = 3.4$. Between aluminum and iron, $n = 3.3$. And between iron and tungsten, $n = 3.1$. These values of n relate only to energies higher than the K-shell potentials.

Figure 1 indicates several things relevant to x-ray dose. First, carbon is the highest-Z material of interest which has no significant absorption edge (i.e., for $E \gtrsim 1$ kev); thus, other materials will behave somewhat differently than carbon and beryllium. Second, for a dispersive spectrum, the effect

---

[2] C. R. Marotta, Updated Master Library Tape for PHOTRAN, Air Force Weapons Laboratory, AFWL-TR-67-11, 1968.

Table 1

COMPUTER-CALCULATED COEFFICIENTS FOR MAXIMUM-DOSE EQUATION

Element	Atomic Number	Coefficient
Beryllium	4	0.20
Carbon	6	0.20
Aluminum	13	0.22
Titanium	22	0.22
Iron	26	0.22
Nickel	28	0.22
Copper	29	0.22
Niobium	41	0.29
Molybdenum	42	0.29
Tungsten	74	0.29

CR79

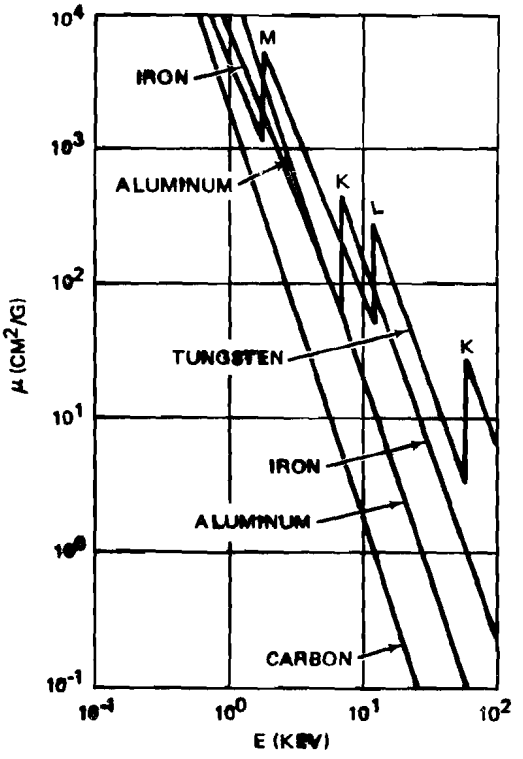

Figure 1. X-Ray Mass Absorption Coefficients

of absorption edges is minimal except for the average absorption coefficient characteristics in terms of effective values of μ_1, m, and n. Third, dose correlations based on the behavior of the absorption coefficient at energies higher than the K-shell potential are not valid for $Z \gtrsim 12$ because of the significant influence of lower energies; the actual dependence on Z and E is weaker than for $m \approx n \approx 3$. Fourth, the effective absorption coefficients have similar behavior only within the three categories of atomic number mentioned above, and in the highest one the effective absorption coefficient is approximately the same for all materials, with the main difference being the individual shell potentials, while their collective effect is nearly identical. Finally, an important property of x-ray absorption coefficients is that they vary smoothly with atomic number, including shell potentials, and therefore integral quantities like doses for dispersive spectra also vary smoothly with atomic number.

Figures 2 through 7 show dose profiles for unit fluence and for 1 to 15 kev blackbody spectra in beryllium, carbon, aluminum, iron, niobium, and tungsten. The maximum dose per fluence at a given depth is represented by the envelope formed by these curves (which is more evident for the higher Z materials). Also shown in the figures are plots of the cumulative fraction of fluence absorbed to a given depth. These data were generated with the previously mentioned computer program. The curves can be interpolated in terms of the effective atomic number (see Equation (10)) and ρx (g/cm^2) to handle any homogeneous material.

It is important to realize that these computer-generated data and any similar data do not represent absolute accuracy. For example, the energy deposition routine in the PUFF code, which uses the mass absorption coefficients of the National Bureau of Standards[3], gives results that in some cases differ by more than a factor of 2 from the data in the figures. This is presumed to be due to a difference in the absorption coefficients.

[3] G. R. White, National Bureau of Standards Report NBS 1003, 1952.

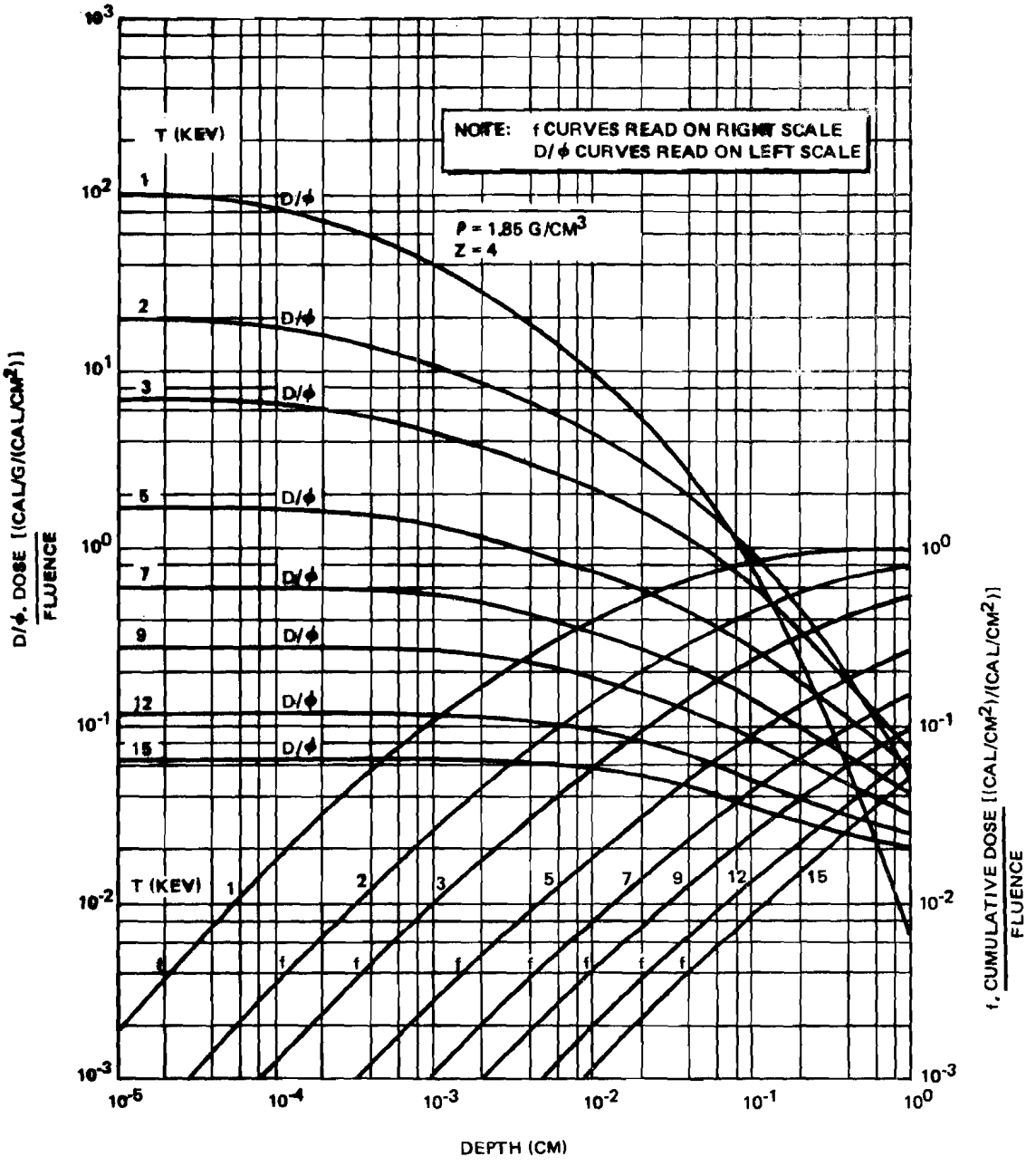

Figure 2. Energy Deposition in Beryllium for Blackbody Spectra

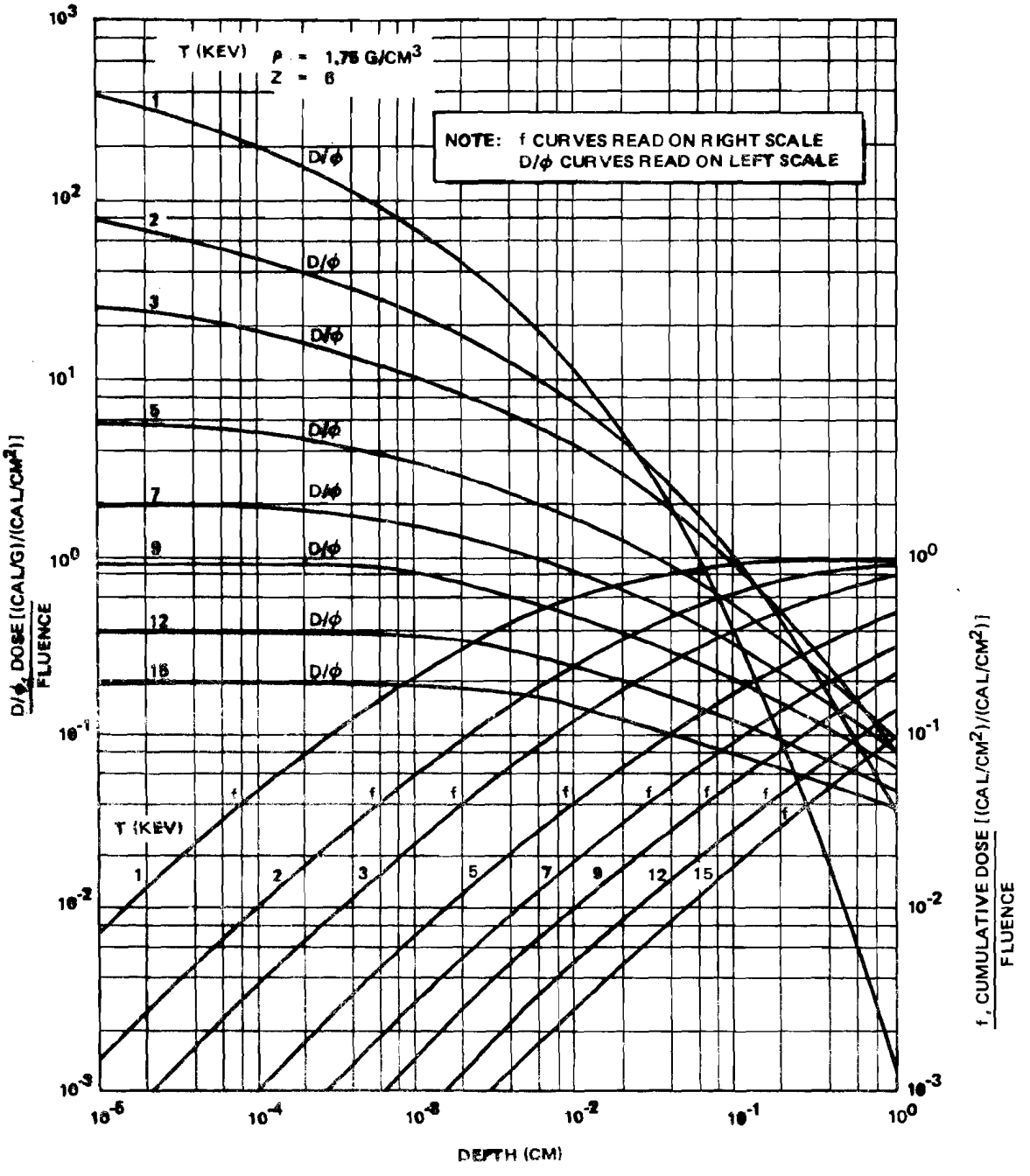

Figure 3. Energy Deposition in Carbon for Blackbody Spectra

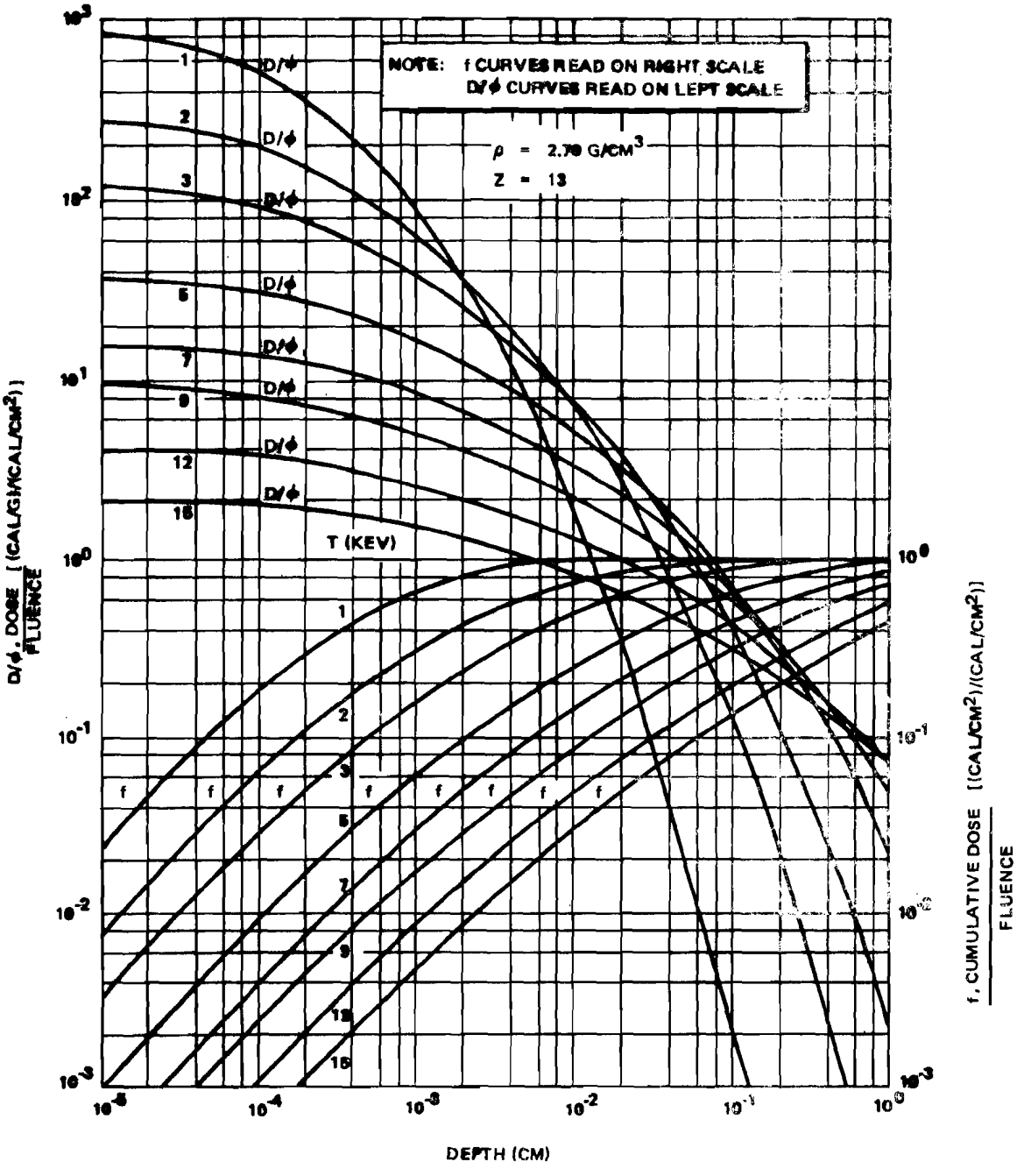

Figure 4. Energy Deposition in Aluminum for Blackbody Spectra

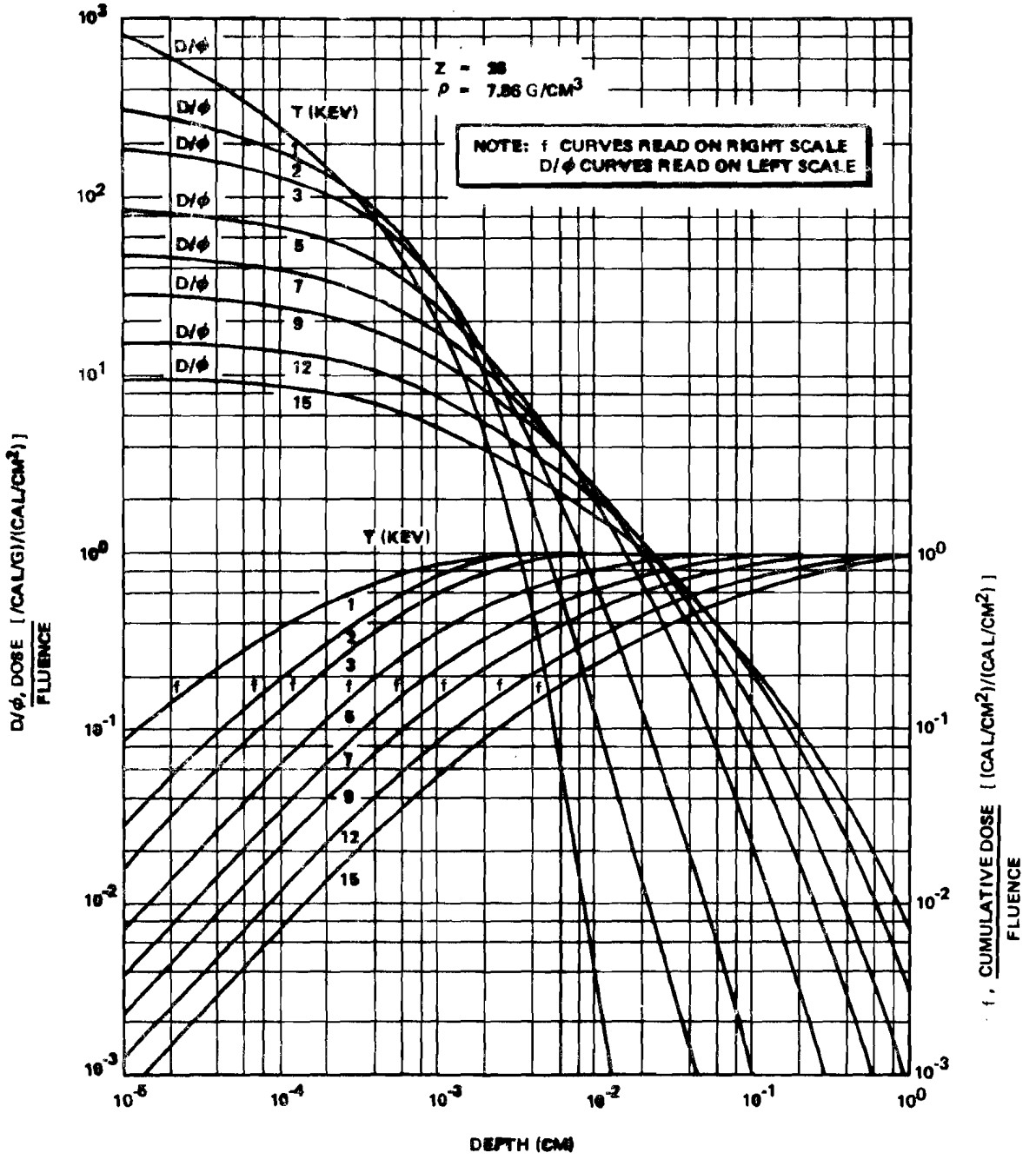

Figure 5. Energy Deposition in Iron for Blackbody Spectra

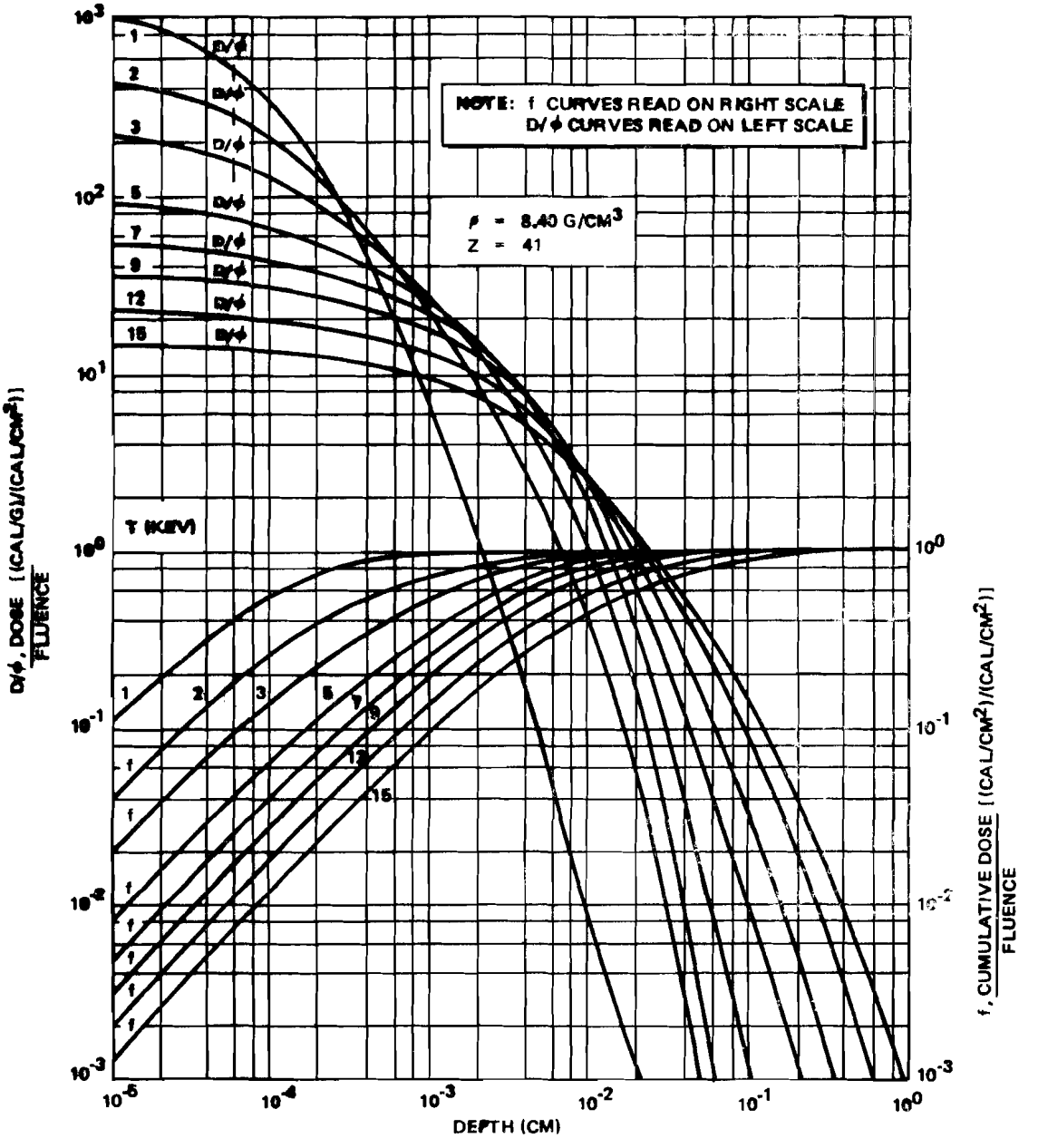

Figure 6. Energy Deposition in Niobium for Blackbody Spectra

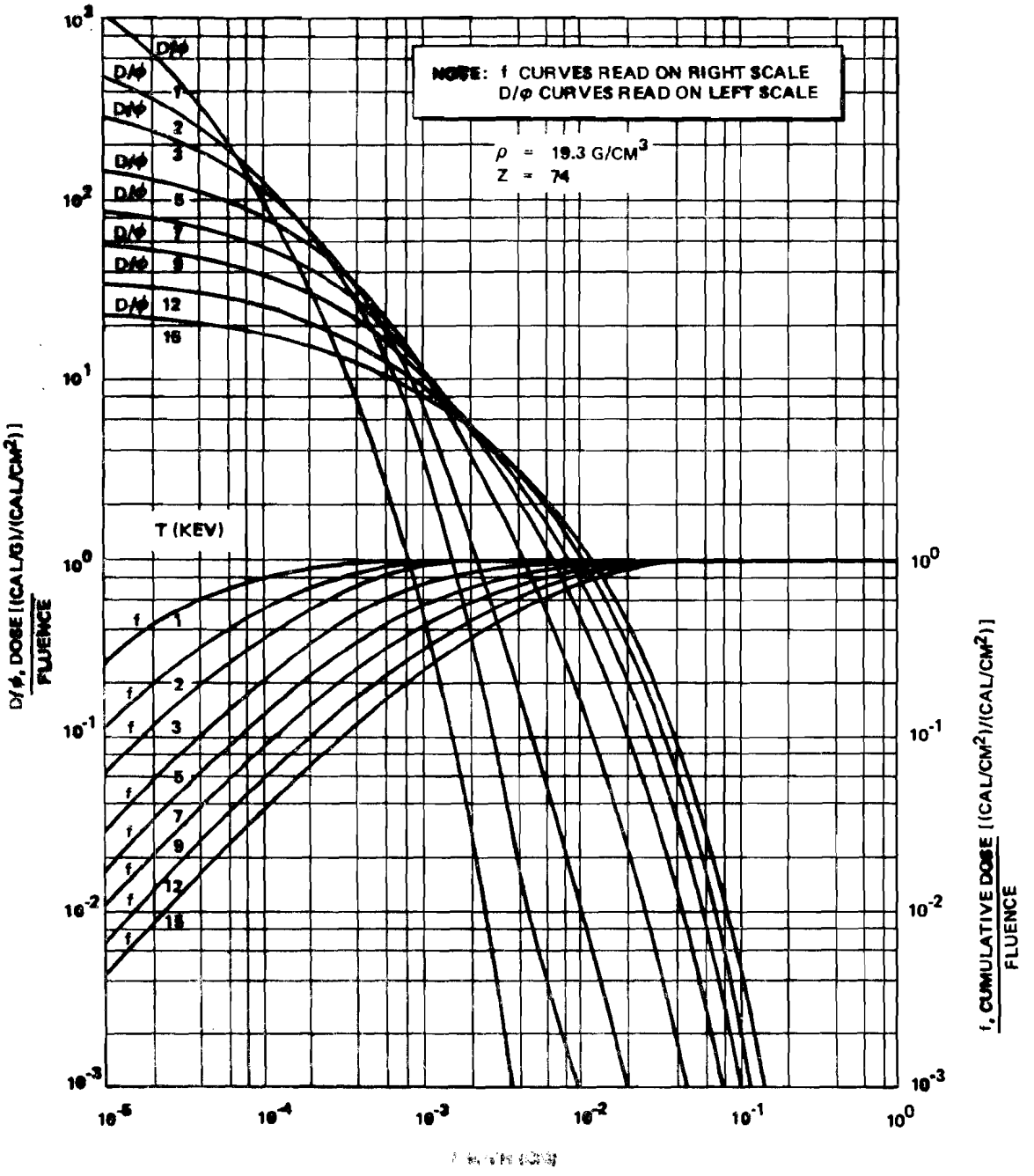

Figure 7. Energy Deposition in Tungsten for Blackbody Spectra

2.1.2 Laminated Materials

For an absorber material of atomic number Z_a and any intervening material (generally called shielding) of atomic number Z_s, which have the same effective values of m and n, Equation (1) leads directly to Equation (6) except for modification by the factor (Z_a^n/Z_s^n) to account for the scaled absorption coefficient as defined by Equation (3).
That is,

$$D_m = 0.24 \frac{\phi}{\rho x}\left(Z_a^n/Z_s^n\right) \tag{7}$$

Parametric computer calculations for $Z_a \leq 30$ and $Z_s \leq 30$, and with $n = 3.3$, compare with Equation (7) to within better than 20 percent.

Because for $Z \geq 40$ the effective absorption coefficient is approximately the same for all materials for the energy range of interest (see Figure 1), parametric computer calculations show that D_m is independent of material for $Z \geq 40$. That is, Equation (6) is also applicable for any combination of materials for $Z \geq 40$ to within better than 20 percent for the materials checked (ranging from niobium to tungsten).

Many parametric computer calculations were made of numerous group 3 materials over numerous group 1 and group 2 materials. Because the effective m's and n's are different for these two categories of materials, energy-dependence and material-dependence are no longer separable, and consequently the functional dependence will be different from the above relationships, requiring an empirical correlation. It was found that for $Z_a \leq 30$ and $Z_s \geq 40$, a simple empirical expression for D_m is

$$D_m = 0.40 \frac{\phi}{(\rho x)^{3/2}}\left(Z_a^n/Z_s^n\right) \tag{8}$$

where $n = 2.8$ and the correlation is within ±40 percent.

Table 2 summarizes the parameters for the general expression

$$D_m = a\phi (\rho x)^{-b} \left(Z_a^n / Z_s^n\right) \tag{9}$$

where a, b, and n are fixed for the material combinations defined in the table. Parameters have not been determined for $Z_a \geq 40$ and $Z_s \leq 30$.

2.1.3 Effective Atomic Number

The above discussion has been in terms of pure elemental materials. However, the relationships have been shown by computer calculations to hold for alloys and composite materials as well. In fact, the above expressions hold for any material or combination of materials if Z, Z_a, and Z_s are each represented by an effective atomic number defined as

$$Z_e = \left(\sum_i w_i Z_i^3\right)^{1/3} \tag{10}$$

where w_i is the mass fraction of each element, and the sum is over all elements in either the shield or the absorber. Whether the shield is a homogeneous material or a laminate is irrelevant. The shield is defined as the total mass of material (in g/cm^2) between the incident radiation and the point at which the dose is evaluated (including air). The value of n = 3 in Equation (10) adequately represents all material combinations for the purpose of determining Z_e; very nearly the same value of Z_e is obtained for $2.8 \leq n \leq 3.3$. Because Z^3 is a strong function, Z_e is usually dominated by one or two elements in a material.

If a laminated "shield" is composed of M different materials whose individual effective atomic numbers are known, a modified version of Equation (10) is convenient for determining the effective atomic number of the shield, Z_{es}

$$Z_{es} = \left(\frac{\rho_1 x_1 Z_{e1}^3 + \rho_2 x_2 Z_{e2}^3 + \cdots + \rho_M x_M Z_{eM}^3}{\rho_1 x_1 + \rho_2 x_2 + \cdots + \rho_M x_M}\right)^{1/3} \tag{11}$$

Table 2

PARAMETERS FOR MAXIMUM - DOSE EQUATION*

Z Range For Shield	Z Range For Absorber	Coefficient a	Z Exponent n	Thickness Exponent b
$Z \leq 30$	$Z \leq 30$	0.24	3.3	1
$Z \geq 40$	$Z \geq 40$	0.24	0	1
$Z \geq 40$	$Z \leq 30$	0.40	2.8	3/2
$Z \leq 30$	$Z \geq 40$	?	?	?
Any Z	$Z_a = Z_s$	0.24	-	1

*General Equation: $D_m = a\phi(\rho x)^{-b}\left(Z_a^n / Z_s^n\right)$

Figure 8 is convenient for relating the Z factor $\left(Z^n \text{ or } Z_e^n\right)$ to the atomic number (Z or Z_e).

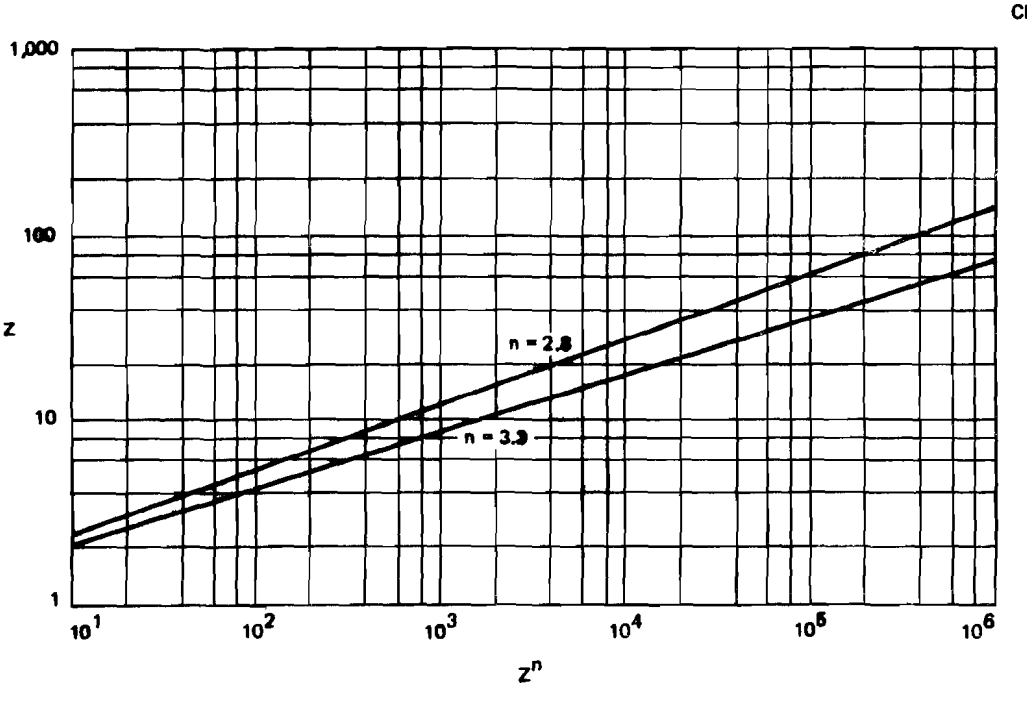

Figure 8. Plot of Z^n versus Z

2.2 DOSE FOR SPECIFIC SPECTRA

For any specific spectrum, an effective general method of dose analysis is based on the above analytical approach. However, it is not completely analytical, but requires a number of dose-versus-depth (in g/cm^2) curves for the range of effective atomic numbers of interest. If specific blackbody spectra are of interest, the parametric curves are like those in Figures 2 through 7, except it is more convenient if the material depth is expressed in g/cm^2 instead of cm.

A conveniently small number of curves can represent the full range of Z_e and T for blackbody spectra; that is, with up to 20 to 30 figures like Figures 2 to 7, a single homogeneous material with a particular Z_e can be adequately represented by the parametric energy-deposition curves of the material with the closest Z_e, without interpolation in Z_e being required. It is important to represent one material by another in terms of g/cm^2 and not in cm to account for differences in density.

For laminated materials, the same procedure is applied to determine the "shield dose," D_s, in the homogenized representation of the shield with effective atomic number Z_{es}. The dose, D_a, in the absorbing material behind the shield is then obtained by scaling D_s by the ratio of Z factors:

$$D_a = D_s \left(Z_{ea}^n / Z_{es}^n \right) \tag{12}$$

Thus, with a set of parametric energy-deposition curves for enough single materials, any material configuration can be easily analyzed. The appropriate values of n for Equation (12) are obtained from Table 2.

2.3 EXPONENTIAL REPRESENTATION OF DOSE PROFILES

2.3.1 Basic Exponential Function

Most actual dose profiles, including those of blackbody spectra, exhibit exponential-like behavior down to a significant degree of dose attenuation. To the extent that an exponential function adequately represents the portion of the dose profile that is dominant for a given effect, closed-form analytical solutions can be obtained for estimating most x-ray effects. This approach was investigated and found to be successful. For optimized quantities

involving the integral of the dose (e.g., blowoff impulse), completely satisfactory results can be obtained even when an exponential function is a poor approximation of the dose profile.

The general representation of dose profiles as an exponential function is

$$D = D_o e^{-\frac{x}{\ell}} \tag{13}$$

where D_o is the surface dose and ℓ is the characteristic dose attenuation depth in cm, or the inverse of the effective (average) linear attenuation coefficient $\bar{\mu}$ (i.e., $\ell = \rho/\bar{\mu}$).

To conserve energy, the integral of Equation (13) over all x must equal the incident fluence. This holds only for an exact exponential profile and results in a unique ℓ which is related to D_o by

$$\ell_o = \frac{\phi}{\rho D_o} \tag{14}$$

However, in some cases (e.g., thermomechanical stress) the quantity to be approximated is not the total energy absorbed, but the initial part of the dose profile. In this case, ℓ is defined as the thickness required to reduce the dose to $e^{-1}D_o$.

Figure 9 shows how the dose profiles for 1, 5, and 15 kev typically vary when divided by D_o and plotted in terms of x/ℓ_o. Also shown are the two kinds of exponential representations for ℓ and ℓ_o, with the areas under the curves indicating energy is not conserved for $\ell \neq \ell_o$. It is seen that $\exp(-x/\ell)$ approximates the actual profile well down to $D/D_o = 0.2$, and underestimates the dose by about a factor of 2 at $D/D_o = 0.1$. Comparisons with computer calculations indicate that this agreement to this degree of attenuation is adequate for predicting x-ray effects for most situations if conservation of energy is introduced when it is important.

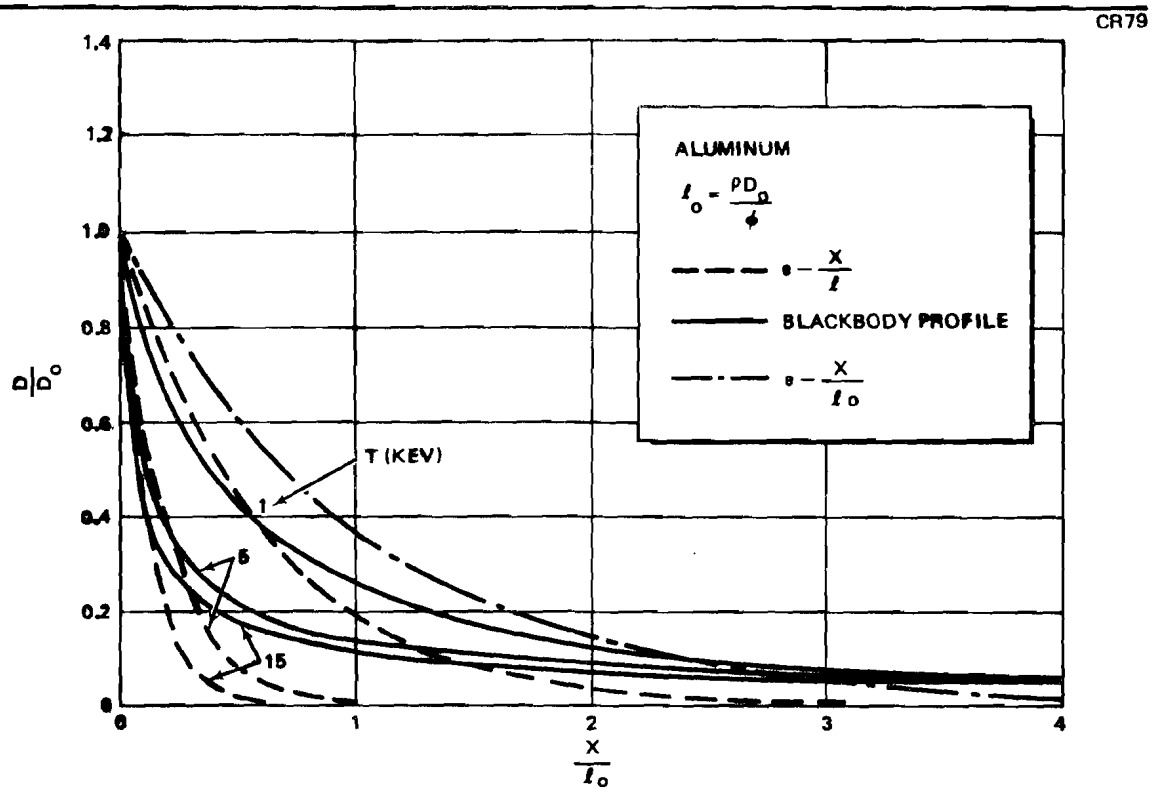

Figure 9. Comparison of Blackbody Dose Profiles with Exponential Approximation

2.3.2 Exponential Parameters for Blackbody Spectra

To apply Equation (13) and relationships which are derived from it to specific blackbody spectra or any other spectra, D_o and ℓ can be obtained from parametric data like those shown in Figures 2 through 7. However, it is useful to have an analytical correlation for D_o and ℓ. Parametric computer calculations were used to determine such expressions empirically for blackbody spectra.

The surface dose is defined by Equation (1) with x = 0. This gives

$$D_o = \phi \int_o^\infty B(E, T)\mu(Z, E)dE = \frac{\phi Z^n}{T^m} \int_o^\infty B(y)\mu_1 \, dy/y^m \qquad (15)$$

For $Z \leq 6$, μ_1 is a constant, $m \simeq 3$, and the integral is a constant. However, for $Z \geq 12$, this is no longer true (see Figure 1), and the integral is a function of Z and T which must be determined empirically. The following relationships were found to correlate all computer-calculated results.

$$D_o = 3\,T^{-3}\,Z^3\phi, \qquad Z \le 6 \tag{16a}$$

$$D_o = 60\,Z\,T^{-2}\phi, \qquad Z \ge 12 \tag{16b}$$

Similarly, the correlations for ℓ are

$$\ell = 0.015\,\frac{T^3}{\rho\,Z^3}, \qquad Z \le 6 \tag{17a}$$

$$\ell = 4 \times 10^{-4}\,\frac{T^{3/2}}{\rho}\left(\frac{Z}{30}\right)^{-1/4} \simeq 4 \times 10^{-4}\,\frac{T^{3/2}}{\rho}, \qquad Z \ge 12 \tag{17b}$$

In these equations, T is in kev, ϕ in cal/cm^2, ρ in g/cm^3, D_o in cal/g, and ℓ in cm.

These correlations were obtained with many claculations using the mass attenuation coefficients of Marotta[2]. Equations (16a) and (17a) reproduce the results to within a few percent. Equations (16b) and (17b) reproduce the results generally to within 30 percent. However, there are a few discontinuities in the calculated data in addition to apparently random scatter, which disagree with the equations by as much as a factor of 2. This is attributed to uncertainties in the mass absorption coefficients, or the numerics of the calculation, or both, since D_o and ℓ must both be smooth functions of Z and E for dispersive spectra. (Several comparisons of Equations (16) and (17) with results obtained with a version of the PUFF computer program, which uses the mass absorption coefficients of the National Bureau of Standards[3], indicate somewhat better agreement than with the Marotta data, but indicate the same general agreement. However, in a few cases the comparison is not as good. It is not known which computer results are best.) Because of the scatter in the calculated data, the approximation of Equation (17) which neglects Z-dependence has the same relative accuracy as when the Z-dependence is retained.

---

[2] Marotta, op. cit.

[3] White, op. cit.

2.4 OPTIMUM TEMPERATURE FOR MAXIMUM DOSE

Because there are always practical limits to the range of blackbody temperatures to be considered, it is necessary to know the optimum temperature corresponding to a particular D_m in order to determine if it is within the range of interest. If it falls outside the range, then the dose and associated quantities are estimated on the basis of the appropriate limiting temperature.

To obtain the optimum temperature T_{op}, D_m is derived for an exponential dose profile. This is done by equating to zero the differential of Equation (13) with respect to ℓ_o, using Equation (14) to relate ℓ_o and D_o. This results in the optimum ℓ_o for an exact exponential profile:

$$\ell_{o\rho} = x \tag{18}$$

and

$$D_m = \frac{e^{-1}\phi}{\rho x} = 0.37\,\frac{\phi}{\rho x} \tag{19}$$

It is first noted that Equation (18) results in Equation (19), which is very similar to Equation (6). However, it cannot be used directly by substituting Equation (17) for ℓ_{op} and solving for T_{op}, nor does it imply that $D_o/D_m = e$, both of which are far from correct. Instead, Equation (18) indicates a general integral relationship for D_m; namely, that for any exponential-like profile, the cumulative fractional energy deposition f, to the depth at which D_m is evaluated, is $f = 1 - e^{-1} = 0.63$. This compares with computer calculations for blackbody spectra to within 10 percent. If $f(e^{-1})$ is approximately constant for a certain class of dose profiles, then so is the total energy balance approximately a constant. Consequently, integrating Equation (13) results in

$$D_o\ell = D_{oe}\ell_o = \frac{D_{oe}\phi}{\rho D_o} \tag{20}$$

where D_{oe} is the surface dose corresponding to an exponential relationship, which in this case is Equation (19), and ℓ_o is related to D_o by Equation (14). Equation (20) is the general expression for equating the total energy of an exponential approximation represented by D_o and ℓ to that for an exponentially derived relationship expressed in terms of D_{oe}. In this case, D_{oe} is given by

$$D_{oe} = eD_m = \frac{\phi}{\rho x} \tag{21}$$

Substituting this into Equation (20) results in

$$D_o^2 \ell = \frac{\phi^2}{\rho^2 x} \tag{22}$$

Substituting Equations (16) and (17) into Equation (22) gives

$$T_{op} = 0.5\, Z\, (\rho x)^{1/3}, \qquad Z \leq 6 \tag{23a}$$

$$T_{op} = 1.2\, Z^{4/5}\, (\rho x)^{2/5}, \qquad Z \geq 12 \tag{23b}$$

Equation (23) is valid for all maximum-dose relationships for which b = 1 (see Table 2). The atomic number of the absorber does not influence T_{op}; the Z in Equation (23) refers to the effective Z of the shield material, i.e., Z_e as defined by Equation (11).

For the maximum-dose relationship of Table 2 for which b = 3/2, a derivation similar to the one given above for T_{op} results in

$$T_{op} = 0.5\, Z^{4/5}\, (\rho x)^{1/2}, \qquad Z \leq 6 \tag{24a}$$

$$T_{op} = 1.2\, Z^{4/5}\, (\rho x)^{3/5}, \qquad Z \geq 12 \tag{24b}$$

In general, the exponent of ρx in Equation (23) scales linearly with b.

The above equations for T_{op} agree within 10 percent to 20 percent (based on graphical data) with parametric computer analysis.

2.5 SUMMARY

The exponential function, Equation (13), as a general operative representation of dose profiles, is presented in the context of x-ray effects analysis. Its relationship to blackbody spectra is described in terms of the surface dose defined by Equation (16), the characteristic dose attenuation depth of Equation (17), and the energy balance relationship of Equation (20). It is used to derive the blackbody temperature corresponding to the maximum dose defined by Equation (9), as expressed by Equations (23) and (24). When dose profiles are needed for $D/D_o \leq 0.2$ for specific blackbody temperatures, parametric energy-deposition data must be used to obtain reasonable accuracy. Dose estimates for specific spectra can generally be determined using parametric energy-deposition data, as described in Section 2.2.

Some of the equations in this and subsequent sections refer to a range of applicable atomic numbers. In general, the atomic number refers to the effective atomic number, Z_e. In cases where a range of Z_e is not covered (e.g., $6 < Z_e < 12$), the situation is undefined, but often the numerical difference between the two equations is not large, so that a choice is not difficult as to whether one of the equations is adequate. If there is insufficient reference to the energy-deposition data or a conservative rationale to make one of the two equations acceptable, one must resort to another approach for these transition situations. While for T_{op} the two equations are very similar for the two ranges of Z_e, so that there is usually not a problem for $6 < Z_e < 12$, Equations (16) and (17) are significantly different for $6 < Z_e < 12$. Therefore, for this range of effective atomic numbers it is usually best to resort to parametric energy-deposition data to determine D_o and ℓ.

Section 3
FRONT-FACE MASS REMOVAL

Mass removal at the front face of a material may involve vaporized, melted, or virgin material. The mass removal plane is always determined by the phenomenon of spall caused by a thermomechanical tensile wave, regardless of the degree of vaporization or melt, or the relative amplitudes of impulse-induced stress and thermomechanical stress.

There are two kinds of criteria for front-face mass removal which are often used to define the spall plane, a dose criterion and a spall threshold criterion. The dose criterion corresponds approximately to the energy required to reach the melt temperature, at which little resistance to a tensile stress wave remains. The spall threshold is usually assumed to be the dynamic strength of the unheated material. Both represent a simplification of the real situation, and a clear choice between the two has not been demonstrated for all situations. Most comparisons have indicated that a dose criterion correlates satisfactorily with experiment for many materials, although there are exceptions, notably graphite.

The modified BBAY model (see Section 5) employs a dose criterion equal to the energy through melt to account for nonvapor mass removal. Mass removal as well as total impulse correlates reasonably well with this criterion for situations involving significant vaporization. Mass removal for metals has been shown to correlate for both x-ray and electron beam dose profiles, with a dose plane corresponding to between one half the melt temperature and the melt temperature. Composite materials like fiber glass have shown a similar correlation. This is not inconsistent with data which show that strength is relatively unaffected by temperature for very short times (see Section 4), at least not until the melt phase is approached. For most structural materials, the energy to melt and the energy through melt, relative to room temperature, differ by only a ratio of 2/3, and often by less.

However, graphite, which is unique in that it has no melt phase and its strength increases with temperature, does not correlate well with a dose criterion. On the basis of existing experimental evidence, a dose criterion is recommended, except for graphitic materials. Using a dose criterion, designated D_r, the maximum thickness of material removed is obtained from Equation (6), and is

$$x_r = 0.24 \frac{\phi}{\rho D_r}$$

where x_r is in cm, ϕ in cal/cm^2, ρ in g/cm^3, and D_r in cal/g. The corresponding optimum blackbody temperature is given by Equation (23). The fraction of the incident fluence absorbed in the remaining thickness of a material is approximated by

$$f = e^{-1} - e^{-\frac{h}{x_r}} \tag{26}$$

where h is the original material thickness in cm (see Sections 2 and 4). This can be used to estimate the average temperature rise of the remaining material in order to evaluate the strength reduction due to the combined effects of mass loss and temperature rise for situations where mass loss is the dominant effect. For the analysis of situations where temperature rise is the dominant effect, see Section 4.

To determine the mass removed for a specific spectrum, the use of parametric energy-deposition data is recommended.

The dose criterion D_r is equal to the energy required to raise the target enthalpy to a certain value. Its numerical value is therefore determined by the ambient temperature of the target material.

Section 4
STRENGTH REDUCTION BY HEATING

One x-ray effect is the heating of exposed load-bearing structures and the consequent reduction in their strength (as well as in the strength of any contiguous bonds). There are two major factors involved in strength loss caused by heating: (1) the removal of mass and the heat capacity and x-ray energy it contains by front-face spall, and (2) the temperature rise of the remaining structure caused by the residual x-ray energy. The first part of the problem is to determine the optimum conditions that will maximize the strength reduction for a given fluence. The second part is to obtain a relationship for estimating the maximum strength reduction.

4.1 OPTIMUM THERMAL CONDITIONS FOR STRENGTH REDUCTION

Generally, strength reduction is a function of the temperature profile across the material thickness. The initial temperature profile created by x-rays is exponential-like, decreasing monotonically with thickness. After a short time (typically on the order of seconds for metals and minutes for composite materials), the profile becomes nearly flat due to thermal conduction. Therefore, the two extremes of temperature profile are the initial profile corresponding to the x-ray energy-deposition profile and the flat quasi-equilibrium profile. The question is what gives the greatest strength reduction.

The three classes of strength-vs.-temperature relationships that characterize most structural materials are shown in Figure 10, where σ_r is the reference strength at or near room temperature, T_t is the threshold temperature where significant strength reduction sets in, and T_m is the melt temperature approximately where the strength goes to zero.

The following generalizations can be shown mathematically for these classes of curves. For a convex curve ($\sigma'' = d^2\sigma/dT^2 < 0$), the optimum temperature profile is flat, with the temperature equal to T_m and the thick-

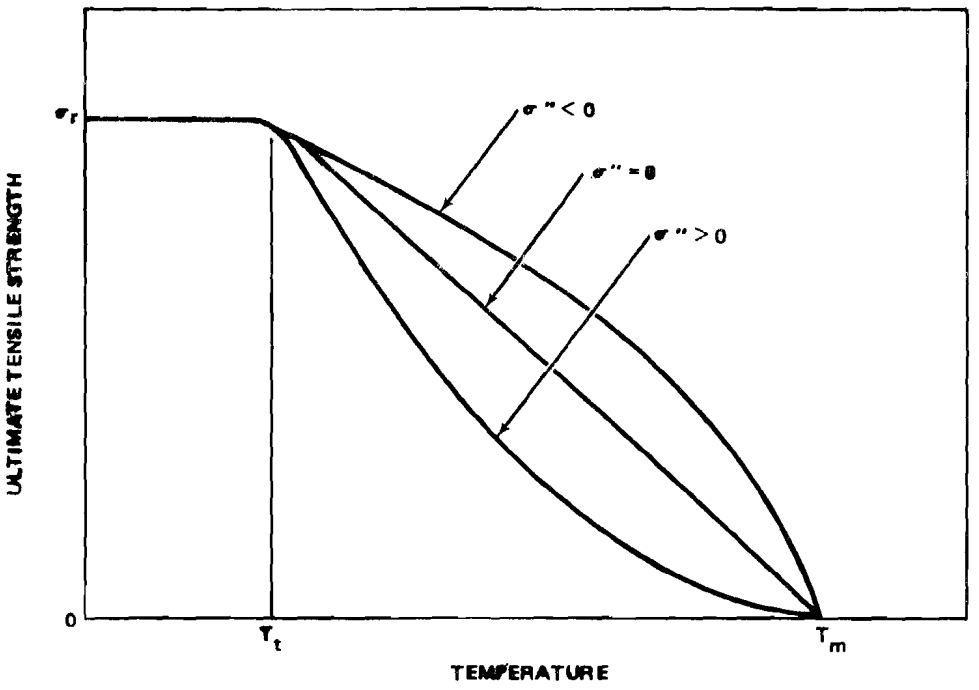

Figure 10. Typical Qualitative Relationships between Strength and Temperature

ness of the heated material corresponding to the amount of energy absorbed. This is approximated by the initial profile. For a concave curve ($\sigma'' > 0$), the optimum profile is flat and extends over the entire thickness of material; i.e., the average or quasi-equilibrium temperature. For a linear curve ($\sigma'' = 0$), the strength reduction is independent of the profile as long as the temperature does not exceed T_m.

Therefore, for convex strength/temperature curves, the optimum temperature profile is the initial energy-deposition profile; otherwise, it is the flat profile corresponding to the average temperature after thermal equilibration.

A more important consideration, however, is that conventional strength/temperature curves are obtained for a heating duration of one half hour while the time regime for x-ray effects is much shorter, on the order of seconds.

Experimental data[4] show that the ultimate tensile strength of 2024 aluminum, 6AL-4V titanium, and 301 stainless steel all drop sharply after rapid heating (by laser), and approach the conventional strength/temperature curve within several seconds. As noted above, this is also the approximate time required for the average temperature to equilibrate in typical structures. These data imply that because the short-term strength reduction with time is far greater than the effect of the temperature profile, strength-reduction estimates for nuclear vulnerability should be based on: (1) conventional strength/temperature curves, and (2) the average, quasi-equilibrium or bulk temperature rather than the initial temperature profile.

Therefore, it is concluded that the optimum thermal condition for strength reduction corresponds to the maximum average bulk temperature rise for a given incident fluence. This is also the most vulnerable situation for the heating of a bond at the rear surface of an exposed material.

4.2 OPTIMUM CONDITIONS FOR HEATING AND MASS REMOVAL

The above conditions consider only temperature effects, given a quantity of absorbed energy. However, optimum conditions must also consider removal of mass due to the significant fraction of absorbed energy that is contains and which is not available for conducting into and heating the remaining material. While the loss of strength of a structure due to the amount of load-bearing material removed can be significant for thin structures, for most realistic situations the synergistic effects of strength reduction due to mass loss and strength reduction due to heating are not important. Thus, optimum mass removal and optimum heating, which occur under different optimum conditions (i.e., different x-ray spectra), can be considered independently, as a reasonable approximation for vulnerability analysis.

Based on the above considerations, the analysis of heating effects can be separated into two essentially independent situations: (1) the situation in which the maximum mass is removed, where this is the primary factor and the accompanying temperature rise is of secondary importance; and (2) the

---

[4] Interaction Study, Vol. IV - Structural Degradation by Short Time Heating, Air Force Weapons Laboratory, AFWL-TR-70-157, Vol. IV. December 1970.

situation in which the maximum temperature rise is the primary factor and mass loss, except as it affects the temperature rise, is of secondary importance. The latter is analyzed here; the other situation is discussed in Section 3.

4.3 MAXIMUM TEMPERATURE RISE

The specific objective is to derive a relationship that defines the maximum temperature rise, accounting for the energy and heat capacity lost by virtue of the mass removed, with the mass removal being determined by a dose criterion.

The temperature rise ΔT, in °C, is given by

$$\Delta T = \frac{\phi}{\rho C_p h} \left(\frac{f - f_r}{1 - x_r/h} \right) \tag{27}$$

where $\phi (f - f_r)$ is the energy absorbed in the remaining thickness of material $(h - x_r)$, ϕ is the incident fluence in cal/cm^2, f is the cumulative fraction of energy absorbed to depth h, f_r is the cumulative fraction of energy absorbed to depth x_r, h is the original thickness in cm, x_r is the thickness in cm of material removed, ρ is the density in g/cm^3, and C_p is the specific heat in cal/g-°C. Assuming an exponential dose profile as a functional approximation to the actual profile,

$$f = 1 - e^{-\frac{h}{\ell}} \tag{28}$$

$$f_r = 1 - e^{-\frac{x_r}{\ell}} \tag{29}$$

and the thickness of material removed is

$$x_r = \ell \ln \frac{D_o}{D_r} = \ell \ln \left(\frac{\phi}{\rho \ell D_r} \right) \tag{30}$$

where ℓ is the characteristic absorption depth in cm, D_o is the surface dose in cal/g, and D_r is the dose criterion in cal/g for mass removal. Combining Equations (29) and (30),

$$f_r = 1 - \frac{\rho \ell D_r}{\phi} \tag{31}$$

Substituting Equations (28), (30), and (31) into Equation (27) gives

$$\frac{\rho C_p h \Delta T}{\phi} = \frac{\frac{\rho h D_r}{\phi} - y e^{-y}}{y - \ell n\, y - \ell n \left(\frac{\phi}{\rho h D_r} \right)} \tag{32}$$

where $y = h/\ell$ has been defined to form a dimensionless spectral parameter.

The objective is to maximize ΔT, which is done by setting the differential of Equation (32) with respect to y equal to zero. This gives

$$y e^{-y} (y-1) \left[y - \ell n y - \ell n \left(\frac{\phi}{\rho h D_r} \right) \right] - (y-1) \left(\frac{\rho h D_r}{\phi} - y e^{-y} \right) = 0 \tag{33}$$

The optimum solution is $y = 1$. The other solution, $y e^{-y} = \rho h D_r / \phi$, defines the limiting conditions where $x_r = h$.

For $y = 1$, $\ell = h$, and Equation (30) becomes for the mass removal,

$$x_r = h \ell n \left(\frac{\phi}{\rho h D_r} \right), \qquad 1 \leq \frac{\phi}{\rho h D_r} \leq e \tag{34}$$

where the range of validity is imposed so that $0 \leq x_r \leq h$. Substituting $y = 1$ into Equation (32) gives for the maximum temperature rise ΔT_m

$$\Delta T_m = \frac{\phi}{\rho h C_p} \left[\frac{\frac{\rho h D_r}{\phi} - e^{-1}}{1 - \ell n \left(\frac{\phi}{\rho h D_r} \right)} \right], \qquad 1 \leq \frac{\phi}{\rho h D_r} \leq e \tag{35a}$$

where the range of validity is taken to be the same as for Equation (34). For the case of no mass removal, $x_r = f_r = 0$ and Equation (27) becomes

$$\Delta T_m = \frac{\phi f}{\rho h C_p} = \frac{\phi}{\rho h C_p}\left(1 - e^{-\frac{\rho h D_r}{\phi}}\right), \qquad \frac{\phi}{\rho h D_r} \leq 1 \tag{35b}$$

Equations (34) and (35) represent the solution for the maximum temperature rise and associated mass removal. They have been compared to parametric computer calculations for blackbody spectra over the full range of parameters and found to give the same result to within better than 10 percent (typically 5 percent).

It is noted that the optimum condition of $\ell = h$ corresponds to the case of maximum dose at the rear surface (see Section 2), regardless of the amount of mass lost. Good agreement is obtained for ΔT_m for blackbody spectra, without modification of the result obtained with an exponential dose profile (as was required for estimating maximum dose), because of the compensation between the factors in Equation (35a) and the insensitivity of Equation (35b) to profile differences.

Figure 11 shows a plot of Equation (35) expressed in dimensionless terms. A somewhat simpler empirical linear equation is found from the figure to represent Equation (35a):

$$\Delta T_m = 0.20\left(\frac{\phi}{\rho h C_p}\right) + 0.43\left(\frac{D_r}{C_p}\right), \qquad 1 \leq \frac{\phi}{\rho h D_r} \leq e \tag{36}$$

Because the optimum temperature rise corresponds to the maximum dose at h, the relationships defining the optimum blackbody temperature for the maximum temperature rise are the same as those of Equation (23) with h substituted for x:

$$T_{op} = 0.5\, Z\, (\rho h)^{1/3}, \qquad Z \leq 6 \tag{37a}$$

$$T_{op} = 1.2\, Z^{4/5}\, (\rho h)^{2/5}, \qquad Z \geq 12 \tag{37b}$$

4.4 SUMMARY

Conditions are defined which maximize strength reduction when both mass removal and heating occur, but when heating is the dominant effect. (See Section 3 for situations when mass removal is the dominant effect.) Because of the importance of strength reduction after rapid heating, the maximum average temperature rise is the parameter that best characterizes the maximum strength reduction. It is given by Equation (35), which is displayed in Figure 11. The optimum blackbody temperature corresponding to the maximum temperature rise is given by Equation (37), and the mass removal is given by Equation (34). For specific blackbody temperatures, x_r and ΔT can be obtained from energy-deposition curve like those shown in Figures 2 through 7.

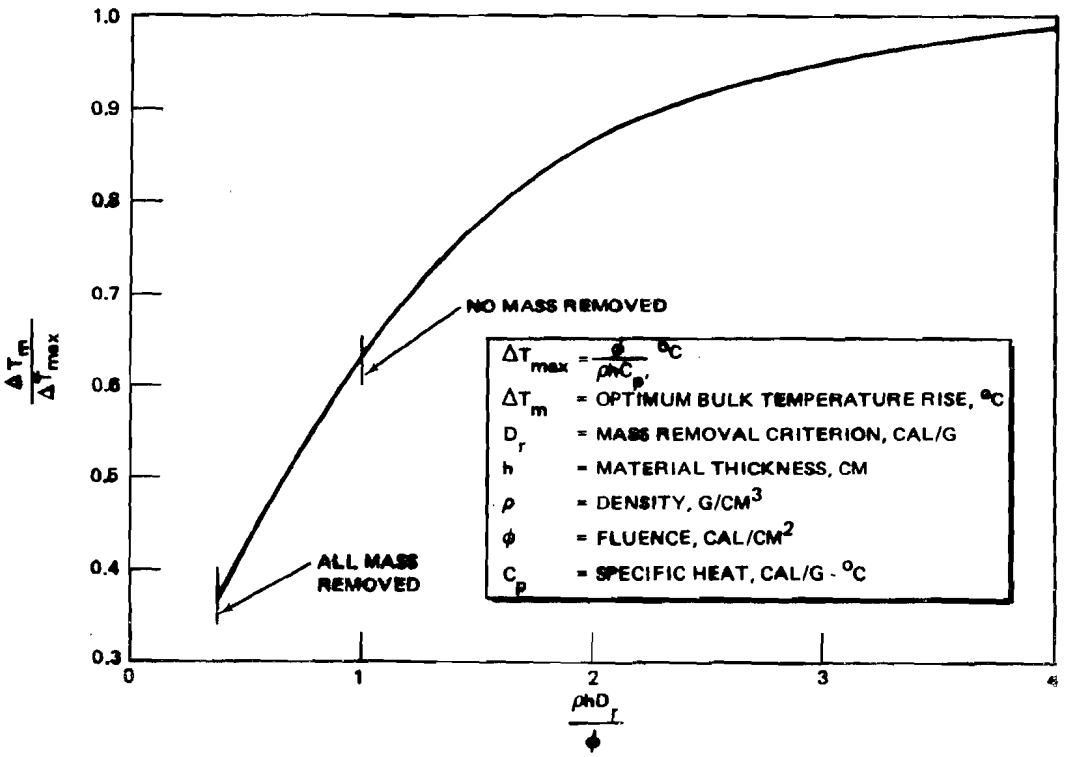

Figure 11. Optimum Bulk Temperature Rise

Section 5

BLOWOFF IMPULSE

When sufficient radiation is rapidly absorbed at the surface of a material, explosive expansion of the vaporized mass creates an impulse load that lasts a few 10's of nonoseconds and can cause damage by material response (e.g., stress wave effects) or structural response. Two models for predicting blowoff impulse have been studied and used extensively. Perhaps still the most popular one is the so-called BBAY model developed by H. A. Bethe et al. for the Air Force Special Weapons Center circa 1962. A modification of the BBAY model was introduced by S. L. Thompson et al. of Sandia Laboratories in 1968. The modified model includes contributions to the impulse from nonvapor phases. The BBAY and the modified BBAY (MBBAY) models are relatively simple relationships, and both compare well with results of PUFF-type analyses which account for hydrodynamic details.

Exact calculations for a general energy-deposition profile using either model are inconvenient because they require a computer program. This section presents generalized curves and explicit relationships which are convenient and are adequate for practical analyses. These relationships are valid for a large class of energy-deposition profiles, including those for blackbody spectra.

5.1 BLOWOFF MODELS

The BBAY model is given by

$$I_B = 1.2 \left[2\rho^2 \int_0^{x_s} (D - E_s) \times dx \right]^{1/2} \qquad (38)$$

where I is the impulse, x_s the thickness of material vaporized, ρ is the density, D is the dose at x, E_s is the effective energy of sublimation (energy through vaporization), and the factor 1.2 is an average value of a weakly varying parameter of the BBAY theory.

For x-rays, energy deposition is taken to be instantaneous so that thermal conduction is neglected. Although it is not necessary, E_s is usually taken to be a constant in Equation (38). However, since it represents an enthalpy change caused by radiation absorption, its value is relative to the initial (reference) temperature of the target material. This can be significant under some conditions. If ionization is significant, the effective E_s can be greater than the reference-temperature E_s; if vapor condensation is significant, it can be less. Accounting for either effect analytically is quite uncertain. Therefore, E_s is taken as a constant and usually assumed to be equal either to the theoretical reference-temperature value at 1 atmosphere pressure, or if available, an experimentally determined (i.e., correlative) value.

The MBBAY model is given by

$$I_M = 1.2 \left\{ 2\rho^2 \int_o^{x_m} \left[D - E_m \left(1 + \ell n \frac{D}{E_m} \right) \right] x \, dx \right\}^{1/2} \tag{39}$$

where E_m is the energy through melt and is used as an approximation to the internal energy at the triple-point state. E_m is influenced by the initial target material temperature in the same way as E_s, but the influence is greater because less energy is involved in phase changes.

5.2 GENERALIZED IMPULSE RELATIONSHIPS

The inconvenience of evaluating Equations (38) and (39) is due to the difficulty of handling analytically complicated energy-deposition profiles like those associated with blackbody x-ray spectra. However, because I is an integral quantity which depends primarily on the 90-percentile portion of the profile

regardless of the fluence level, it is insensitive to the form of the profile, especially for thicknesses for which D is less than 10 percent of the surface dose. Consequently, Equations (38) and (39) can be evaluated by assuming the functional form of D to be

$$D = D_o e^{-\frac{x}{\ell}} \tag{40}$$

where D_o is the surface dose and ℓ is the characteristic absorption depth.

Substituting Equation (40) into Equation (38) and integrating gives for BBAY

$$\frac{I_B}{I_{B_{max}}} = 3.34 \left\{ \frac{2}{\eta} \left[1 - \frac{1}{\eta} (1 + \ell n \eta) \right] - \left(\frac{1}{\eta} \ell n \eta \right)^2 \right\}^{1/2} \tag{41}$$

where

$$I_{B_{max}} = \frac{2.3\phi}{E_s^{1/2}} \tag{42}$$

and

$$\eta = \frac{D_{oe}}{E_s} \tag{43}$$

where D_{oe} indicates the surface dose for an exact exponential dose profile.

Similarly, Equation (39) gives for MBBAY

$$\frac{I_M}{I_{M_{max}}} = 4.99 \left\{ \frac{2}{\eta} \left[1 - \frac{1}{\eta} (1 + \ell n \eta) \right] - \left(\frac{1}{\eta} \ell n \eta \right)^2 - \frac{\eta}{3} \left(\frac{1}{\eta} \ell n \eta \right)^3 \right\}^{1/2} \tag{44}$$

where

$$I_{M_{max}} = \frac{1.6\phi}{E_m^{1/2}} \tag{45}$$

and

$$\eta = \frac{D_{oe}}{E_m} \tag{46}$$

In these equations, I is in kilotaps, ϕ is the fluence in cal/cm^2, and E_s, E_m, and D_{oe} are in cal/g. E_s and E_m are threshold doses designated generally as E_t. These equations are presented here as general representations of the BBAY and MBBAY models for exponential-like dose profiles, and as being adequate for blowoff impulse analysis. Although the actual derivation of the these equations is not new, their general validity and specific relationship to blackbody spectra, as described in this section, is unique.

5.3 APPLICATION TO EXPONENTIAL-LIKE DOSE PROFILES

Since conservation of energy is important for blowoff impulse just as it is for maximum dose, application of the exponentially derived relationships to other similar dose profiles requires the use of the energy balance derived in Section 2. From an energy balance, Equation (20) defines D_{oe} as

$$D_{oe} = \frac{\rho \ell D_o^2}{\phi} \tag{47}$$

Therefore, η is defined generally as

$$\eta = \frac{D_{oe}}{E_t} = \frac{\rho \ell D_o^2}{\phi E_t} \tag{48}$$

where D_o and ℓ are parameters representing any particular dose profile, as described in Section 2. Consequently, to apply Equations (41) and (44) to any exponential-like spectrum requires only a knowledge of the corresponding D_o and ℓ for that spectrum.

Analytical expressions for D_o and ℓ are given by Equations (16) and (17) for blackbody spectra. They result in:

$$\eta = 0.14 \frac{Z^3 \phi}{T^3 E_t} , \quad Z \leq 6 \tag{49a}$$

$$\eta = 1.4 \frac{Z^2 \phi}{T^{5/2} E_t} , \quad Z \geq 12 \tag{49b}$$

5.4 DISCUSSION OF EQUATIONS

Equations (41) and (44) are plotted in Figure 12 with η defined by Equation (48). They are very similar except for a shift in the optimum value of η, which is 6.00 for BBAY and 10.2 for MBBAY. The optimum value, η_o, defines the optimum energy spectrum, but as shown in the figure, the optimum is broad and relatively insensitive to the spectrum (which may or may not be characterized by a blackbody temperature).

From Equations (42) and (45) and Figure 12, it is apparent that the maximum impulse for a given fluence, corresponding to the optimum spectrum, is easily obtained and requires a knowledge only of ϕ and E_t, if the optimum spectrum falls within the environment specifications. This is usually the case and represents most practical situations (except for beryllium and carbon). If the optimum temperature falls outside the specified spectral range, only the actual D_o and ℓ for the limiting temperature is necessary in addition.

As far as contrasting the two blowoff models is concerned, one difference is that the optimum blackbody temperature can be as much as a factor of

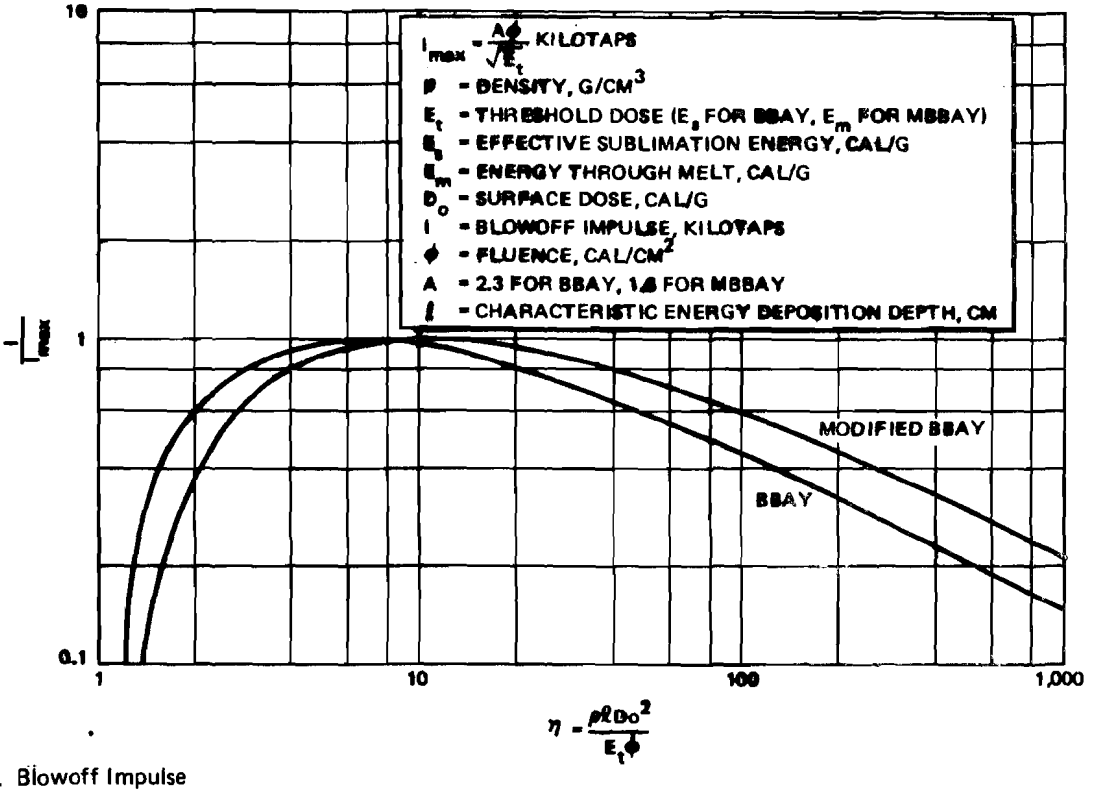

Figure 12. Blowoff Impulse

2 greater for MBBAY than for BBAY. The flat optimum indicated in Figure 12 and its application to a range of spectra tend to make the difference in optimum conditions of little practical significance. The other difference in the two models is that the maximum impulse differs by

$$\frac{I_{M_{max}}}{I_{B_{max}}} = \left(\frac{1.6}{2.3}\right)\left(\frac{E_s}{E_m}\right)^{1/2} = 1.4 \pm 20\% \qquad (50)$$

Parametric computer calculations for blackbody spectra indicate that Equation (50) is valid for most materials (i.e., all the various materials that were checked). Therefore, practically speaking (i.e., within 20 percent), BBAY and MBBAY are interchangeable except MBBAY is approximately 1.4 times higher. The exceptions to this will be for materials for which E_s/E_m is greater than 6.

5.5 OPTIMUM CONDITIONS FOR MAXIMIZING IMPULSE

As noted earlier, general optimization of impulse is obtained from Figure 12 in terms of η_o for a large class of dose profiles. This section discusses techniques for handling blackbody spectra specifically.

Combining Equation (49) with $\eta_o = 6$ for BBAY and $\eta_o = 10.2$ for MBBAY results in the optimum blackbody temperature for maximum blowoff. For BBAY,

$$T_{OB} = 0.29\, Z \left(\frac{\phi}{E_s}\right)^{1/3}, \quad Z \le 6 \tag{51a}$$

$$T_{OB} = 0.62\, Z^{4/5} \left(\frac{\phi}{E_s}\right)^{2/5}, \quad Z \ge 12 \tag{51b}$$

and for MBBAY,

$$T_{OM} = 0.24\, Z \left(\frac{\phi}{E_m}\right)^{1/3}, \quad Z \le 6 \tag{52a}$$

$$T_{OM} = 0.52\, Z^{4/5} \left(\frac{\phi}{E_m}\right)^{2/5}, \quad Z \ge 12 \tag{52b}$$

Since for a variety of materials $(E_s/E_m)^{2/5} = 2 \pm 20\%$, $T_{OM} \simeq 1.5\, T_{OB}$ for $Z \le 6$ and $T_{OM} \simeq 1.7\, T_{OB}$ for $Z \ge 12$.

For a given fluence, Equation (51) or (52) can be used to determine whether the optimum temperature is within the range of temperatures to be considered. If it is, Equation (42) or (45) is used. Otherwise, D_o and ℓ for the limiting temperature, along with Equation (41) or (44) or Figure 12, is used to determine the maximum impulse under the imposed conditions. In fact, for any specific nonoptimum temperature, the latter procedure is applicable.

5.6 MAXIMUM BLOWOFF IMPULSE IN SHIELDED MATERIALS

The maximum blowoff impulse in a material shielded by air or by a non-contiguous structure like a shroud can be obtained by observing in Figure 12 that the maximum impulse corresponds to the maximum η up to $\eta = \eta_o$. For $\eta > \eta_o$, this is still a good approximation for most realistic situations. The maximum η is shown to correspond to the maximum D_o, as follows.

The maximum dose is given by Equation (7), which is set equal to D_o:

$$D_m = D_o = \frac{0.24}{\rho_s x_s} \left(Z_a^n / Z_s^n \right) \tag{53}$$

where subscript s refers to the shielding material and subscript a to the absorber or target material. In addition to the integral relationship discussed in Section 2, Equation (18) indicates that at depth x the optimum effective linear attenuation coefficient is equal to x (see Figures 2 through 7). Using Equations (18) and (53) gives

$$\ell_s = x_s = \frac{0.24\phi}{\rho_s D_o} \left(Z_a^n / Z_s^n \right) \tag{54}$$

The linear attenuation coefficients for the shield and target are related by

$$\frac{\rho_s \ell_s}{\rho_a \ell_a} = \left(Z_a^n / Z_s^n \right) \tag{55}$$

So that combining Equations (54) and (55) gives

$$\ell_a = \frac{0.24\phi}{\rho_a D_o} \tag{56}$$

Substituting Equations (53) and (56) into Equation (48) gives the maximum η for a shielded target:

$$\eta_s = 0.24\frac{D_o}{E_t} = \frac{0.06\phi}{\rho_s x_s E_t}\left(Z_a^{3.3}/Z_s^{3.3}\right), \quad b = 1 \tag{57a}$$

where b is the thickness exponent of Table 2, and the appropriate value of n = 3.3 has been shown. A similar derivation gives

$$\eta_s = 0.27\frac{D_o}{E_t} = \frac{0.11\phi}{(\rho_s x_s)^{3/2}E_t}\left(Z_a^{2.8}/Z_s^{2.8}\right), \quad b = 3/2 \tag{57b}$$

and in general,

$$\eta_s = \frac{a^2\phi}{E_t b}(\rho_s x_s)^{-b}\left(Z_a^n/Z_s^n\right) \tag{58}$$

where the fact that $\ell_s = -(d\ell nD_m/dx)^{-1} = x_s/b$ has been used.

Thus, Equation (57) shows that the maximum η is directly proportional to the maximum D_o. Therefore, for a given shielding mass of $\rho_s x_s$ (g/cm^2), Equation (57) is used to obtain η_s, which is used with Figure 12 to derive maximum impulse. For the analytical model used here, this optimization is exact for $\eta \le \eta_o$ and is a good approximation for $\eta > \eta_o$.

In Equation (57), ϕ is not the fluence incident on the target, but the fluence that would be incident if there were no shielding material. This formulation makes it possible to retain the concept of a blackbody source. The blackbody source temperature corresponding to Equation (57) is given by Equation (23) or Equation (24), depending on the value of b.

5.7 REVIEW OF COMPARISONS WITH EXPERIMENT

Both blowoff models have been compared extensively with experimental data, some published, especially by the Air Force Weapons Laboratory and Sandia Laboratories, and some unpublished. The general indication is that

both models compare to within a factor of 2, with the MBBAY model appearing to be slightly better. Since the uncertainty in the experimental data is about a factor of 2, no clear choice is indicated.

On the other hand, the BBAY model correlates better than the MBBAY model with blowoff impulse caused by high-energy pulsed lasers.[5] Experimental laser blowoff impulse data cover a larger range of η and characteristic absorption depths than do x-rays because thermal conductivity becomes an effective energy transport mechanism as beam pulse widths increase from picoseconds to milliseconds. Also, blowoff data for lasers are significantly more accurate and better correlated than for x-rays. The laser data correlate well with the BBAY model over a variety of materials and for a large range of fluences and beam pulse widths (the effect of beam pulse width being analogous to blackbody spectrum), but the BBAY model gives results that are consistently higher than those obtained by experiment by a factor of 1.5 to 2. Also, laser data indicate that the effective E_s is slightly greater than the room-temperature value, while test data indicate the opposite for x-rays.

The conclusion is that either model can be justifiably used, especially since nothing better is available, and the matter is largely one of personal preference since the results they give are quite similar. For the MBBAY model, however, E_m values are less ambiguous than the effective E_s values for the BBAY model, and they are available for more materials. Further, the MBBAY model gives more conservative estimates from a system design standpoint. Also, the use of E_m by the MBBAY model for a threshold energy is more consistent with other data relating to front-face mass removal.

5.8 SUMMARY

For almost any radiation source, Equations (41), (42), (44), and (45) give blowoff impulse estimates that are more accurate than the demonstrated accuracy of the BBAY and MBBAY models, as determined by comparison

---

[5] R. W. Langley, "An Analytic Model for Laser Blowoff Impulse," McDonnell Douglas Paper No. WD 2408, June 1974.

with parametric computer calculations. Equations (42) and (45) compare with detailed computer calculations for blackbody spectra generally to within 10 percent, with no more than 20 percent difference, for fluences to greater than 10^3 cal/cm^2. Figure 12 has been compared for non-optimum situations only for the BBAY model. For extremely high fluences ($\eta \simeq 1{,}000$), the comparison is better than 30 percent. For low fluences, the agreement is similar except where very little vaporization occurs. However, this regime is narrow, is inherently uncertain in any case, and is of relatively little importance from a practical standpoint. Equations (51) and (52) compare with computer calculations to within about 20 percent.

The relationships given here are recommended for blowoff impulse analysis. The equations are depicted in Figure 12. The MBBAY model is slightly favored over the BBAY model because it gives slightly larger impulses and has a better defined energy threshold in E_m.

The only quantities needed to define the incident radiation source are ϕ, D_o, and ℓ. Methods for determining optimum conditions for maximum impulse are discussed in Section 5.5.

Section 6
STRESS GENERATION

Stress waves generated by radiation fall into two categories: (1) those induced by blowoff impulse, and (2) thermomechanical stress waves. The two types always occur to some extent concurrently, but for most practical situations only the maximum of one or the other is of interest. Generally, when impulse-induced stresses are maximized for a given fluence, thermomechanical stresses are negligible, and conversely when thermomechanical stresses are maximized, impulse-induced stresses are negligible — in fact, they are zero. Which of the two is dominant for a given situation is determined by the radiation spectrum. Therefore, for the optimum conditions, the two types of stresses and their associated damage mechanisms are analyzed independently. In some situations, combined stresses may be of interest. Analytical techniques for estimating stress generation (i.e., initial stress conditions near the material surface exposed to radiation) are discussed below. Attenuation of stresses as they propagate through a material is discussed in Section 7.

6.1 IMPULSE-INDUCED STRESSES

A blowoff impulse, I, is characterized by an average initial pressure or stress amplitude σ_o with a temporal pulse width τ, so that

$$\sigma_o = \frac{I}{\tau} \tag{59}$$

where σ_o is in kilobars, τ is in microseconds, and I is in kilotaps. The value of τ is determined either by the energy-deposition time or radiation shine time τ_s, or by τ_g, the time required for the vaporized gas to expand, whichever is greater.

An estimate of τ_g is obtained from

$$\tau_g \simeq \frac{3\ell}{C_g} \tag{60}$$

where ℓ is the characteristic radiation absorption depth in cm and C_g is the acoustic velocity of the vapor in cm/μsec. The thickness of vaporized mass is approximated by 3ℓ, which corresponds to the mass in which most of the energy is absorbed. The acoustic velocity is given by

$$C_g = \left(\frac{\gamma \sigma_o}{\rho_g}\right)^{1/2} \tag{61}$$

where the specific heat ratio γ is 5/3 for a monoatomic gas and ρ_g is the density of the vapor. For a pressure of σ_o, the vapor density is the same as the solid density; i.e., $\rho_g = \rho$. Combining Equations (59) through (61) gives for τ_g

$$\tau_g = 5400\rho\ell^2/I \tag{62}$$

where τ_g is in microseconds, ρ is in g/cm^3, ℓ is in cm, and I is in kilotaps. The value of ℓ can be obtained from an energy-deposition profile (e.g., Figures 2 to 7) or it can be estimated for blackbody spectra from Equation (17). For $Z \geq 12$,

$$\ell = 4 \times 10^{-4} \frac{T}{\rho}^{3/2} \tag{63}$$

where ℓ is in cm, T is in kev, ρ is in g/cm^3, and Z is the material (effective) atomic number.

Substituting Equation (63) into Equation (62) gives, using the same units,

$$\tau_g = 9 \times 10^{-4} \frac{T^3}{\rho I} , \quad Z \geq 12 \tag{64}$$

In general, then, σ_o is determined from Equation (59) by using the largest value of τ corresponding either to the shine time τ_s or to τ_g as given by Equations (62) or (64).

For maximum blowoff impulse for the BBAY blowoff model, however, the corresponding optimum temperature for $Z \geq 12$ is given by

$$T_{OB} = 0.62 Z^{4/5} \left(\frac{\phi}{E_s} \right)^{2/5} \tag{65}$$

where ϕ is the fluence in cal/cm^2 and E_s is the effective sublimation energy of the material in cal/g. Inserting Equation (65) into Equation (64) gives τ_g for maximum blowoff impulse for $Z \geq 12$; a similar derivation applies to $Z \leq 6$. The results are:

$$\tau_{go} = 2 \times 10^{-4} \frac{Z^{12/5}}{\rho I} \left(\frac{\phi}{E_s} \right)^{6/5} , \quad Z \geq 12 \tag{66a}$$

$$\tau_{go} = 6 \times 10^{-4} \frac{\phi^2}{\rho I E_s^2} , \quad Z \leq 6 \tag{66b}$$

Equation (66) shows that for maximum blowoff impulse, $\tau_{go} < 0.02$ microsecond for most practical situations, and thus $\tau = \tau_s$ for these cases. For example, for $I > 1/2$ kilotap, $\tau_{go} < 0.02$ microsecond for $\phi < 70$ cal/cm^2, for all materials (ϕ is lowest for tungsten). For carbon and beryllium, $\tau_{go} < 0.02$ for $\phi < 10^4$ cal/cm^2.

The initial spatial pulse width δ_o, which is used in conjunction with σ_o as initial conditions for analyzing stress wave attenuation, is given by

$$\delta_o = 2C\tau \tag{67}$$

where C is the acoustic velocity of the solid. The factor of 2 is introduced in order to express the square wave represented by Equation (59) as a triangular wave form, which is the equilibrium shape to which all initial pulses degenerate as they propagate.

6.2 THERMOMECHANICAL STRESSES

Thermomechanical stresses are caused by the forces associated with the thermal expansion of a material when it is rapidly heated internally by radiation. This section considers only situations involving no front-face mass removal. Because there is no net impulse in these situations, a thermomechanical stress wave always consists of a compressive wave followed by a tensile wave of equal but opposite impulse. The tensile wave that immediately forms near the surface of an exposed material (and can cause fracture, spall, or debonding) is the main difference between thermomechanical stresses and compressive blowoff stresses, which can form a tensile stress only by reflecting at an inner boundary.

For instantaneous energy deposition, the initial stress is compressive and has the same shape as the dose profile, and the peak stress is determined only by the maximum dose at the surface. However, for a finite shine time, the peak stress is reduced significantly below that for an instantaneous exposure at the same fluence, and therefore shine-time effects must be accounted for.

6.2.1 Stresses for Instantaneous Energy Deposition

Linear-elastic behavior is assumed and the dose profile is represented by an exponential function. Conservation of energy is not important, but an accurate represenatation of the initial portion of the dose profile is of concern. With the dose profile represented by

$$D = D_o e^{-\frac{x}{\ell}} \tag{68}$$

Morland[6] gives the compressive stress to be

$$\sigma_{co} = 0.042\ \rho\Gamma D_o e^{-\frac{x}{\ell}} \cosh\frac{Ct}{\ell}\ , \qquad x \geq Ct \tag{69}$$

and the tensile stress to be

$$\sigma_{to} = 0.042\ \rho\Gamma D_o e^{-\frac{Ct}{\ell}} \sinh\frac{x}{\ell}\ , \qquad x \leq Ct \tag{70}$$

where 0.042 is the conversion factor between cal/cm^3 and kilobars, D_o is the surface dose in cal/g, x is the depth into the material in cm, Γ is the dimensionless Gruneisen coefficient, t is the time after exposure in microseconds, and the stresses are in kilobars.

At t = 0, $\sigma_{to}(0) = 0$ and $\sigma_{co}(0) = 0.042\ \rho\Gamma D(x)$. Equilibrium stresses exist for $Ct \gtrsim 3\ell$, for which $\sigma_{co}(\infty) = 1/2\ \sigma_{co}(0)$ and $\sigma_{to}(\infty)$ is the same shape and magnitude as $\sigma_{co}(\infty)$, but is oriented in the opposite direction.

The exact expression for the positive impulse of the equilibrium compressive stress wave, expressed in kilotaps, is

$$I_c = 1/2 \int_o^\infty \sigma_{co} \frac{dx}{C} = 0.021 \frac{\rho\Gamma D_o \ell}{C} = 0.021 \frac{\Gamma\phi}{C} \tag{71}$$

where $\rho \ell D_o = \phi$ has been used in deriving the final expression because it represents conservation of energy, and is valid in this context. The negative impulse of the equilibrium tensile stress is also given by Equation (71), since the sum of both impulses is zero.

---

[6] L. W. Morland, Generation of Thermoelastic Stress Waves by Impulsive Electromagnetic Radiation, AIAA Journal, Vol. 6, No. 6, pp 1063-1066, June 1968.

Although the impulse does not change with finite shine time, the peak equilibrium stresses are reduced considerably for typical values of ℓ because the stress relaxes during the shine time.

6.2.2 Shine-Time Effect

For a constant radiation flux during a shine time τ, the compressive stress for $t \leq \tau$ is given by convolution of Equation (70):

$$\sigma_c = \int_0^t \sigma_{co}(t') \frac{dt'}{\tau} = 0.042 \frac{\rho\Gamma D_o \ell}{C\tau} e^{-\frac{x}{\ell}} \sinh \frac{Ct}{\ell} , \quad x \geq Ct \tag{72}$$

Equation (72) shows that the peak initial compressive stress occurs at $t = \tau$ and $x = C\tau$, and that the reduction factor for the peak stress is

$$\frac{\sigma_{c(\tau)}}{\sigma_{co}(0)} = \frac{\ell}{2C\tau}\left(1 - e^{-\frac{2C\tau}{\ell}}\right) \tag{73}$$

Equation (73) represents the effect of shine time in reducing the peak initial compressive stress. This same factor also applies to the reduction of the peak equilibrium (i.e., $Ct = x \gg \ell$, $t \gg \tau$) tensile and compressive stresses since they are both one half the magnitude of the peak initial compressive stress.

6.2.3 Maximum Peak Equilibrium Stress

The peak equilibrium stress that exists for $x \gtrsim 3\ell$ is the main quantity of interest, especially the peak equilibrium tensile stress. When a range of radiation spectra is considered, the maximum peak stress for the optimum spectrum may be desired. Maximizing peak stress for a given fluence corresponds to maximizing $D_o \ell$, which minimizes the shine-time effect while maximizing the surface dose, but with the constraint that front-face mass removal is avoided.

The peak equilibrium tensile or compressive stress for instantaneous energy deposition is, from Equations (69) and (70).

$$\sigma_{op} = 0.021 \rho\Gamma D_o \tag{74}$$

where $Ct = x \gg \ell$. Combining Equations (73) and (74) gives the peak equilibrium tensile or compressive stress for finite τ:

$$\sigma_p = 0.01 \frac{\rho \Gamma D_s \ell}{C\tau} \left(1 - e^{-\frac{2C\tau}{\ell}}\right) \tag{75}$$

where D_s is the dose at the surface of the solid material, and is equal either to D_o, the surface dose of Equation (68), or to D_r, the mass removal criterion, whichever is smaller. That is,

$$D_s = \text{MIN} \begin{cases} D_o \\ D_r \end{cases} \tag{76}$$

Equation (75) is the general equation for peak stress for any exponential-like dose profile. It compares closely with computer calculations for blackbody spectra.

To obtain the maximum peak equilibrium stress, Equation (75) must be optimized. As already noted, for an exponential profile, the integral relationship holds that $\rho \ell D_o = \phi$. However, parametric computer calculations show that for blackbody spectra there is a maximum value for $\rho \ell D_o$:

$$\text{Max}\,(\rho D_o \ell) = k\phi \tag{77}$$

where $k = 0.05$ for $Z \leq 6$ and $k = 0.6$ for $Z \geq 12$. The maximum values are a function of T and Z for $Z \geq 12$, with optimum T varying from 2 kev for aluminum to 5 kev for tungsten. (While a constant k is correct, it may be noted that it is somewhat inconsistent with the empirical expressions for D_o and ℓ for $Z \geq 12$.)

Using a dose criterion D_r to determine mass removal, Equation (77) gives for the optimum ℓ consistent with no mass removal (i.e., $D_s = D_o = D_r$),

$$\ell_m = \frac{k\phi}{\rho D_r} \tag{78}$$

Combining Equations (75), (77), and (78) gives the maximum peak equilibrium tensile or compressive stress, for any fluence, for blackbody spectra:

$$\sigma_{pm} = 0.01 \frac{k\Gamma\phi}{C\tau} \left(1 - e^{-\frac{2\rho D_r C\tau}{k\phi}}\right) \tag{79}$$

Equation (79) is plotted in Figure 13 in dimensionless terms. The surface dose always equals D_r. It is noted that Equation (79), except for k, is insensitive to material variations since Γ, C, and D_r are approximately the same for many materials.

Combining Equations (17) and (78) gives for the optimum blackbody temperature corresponding to Equation (79):

$$T_{op} = 1.5\, Z \left(\frac{\phi}{D_r}\right)^{1/3}, \qquad Z \leq 6 \tag{80a}$$

CR79

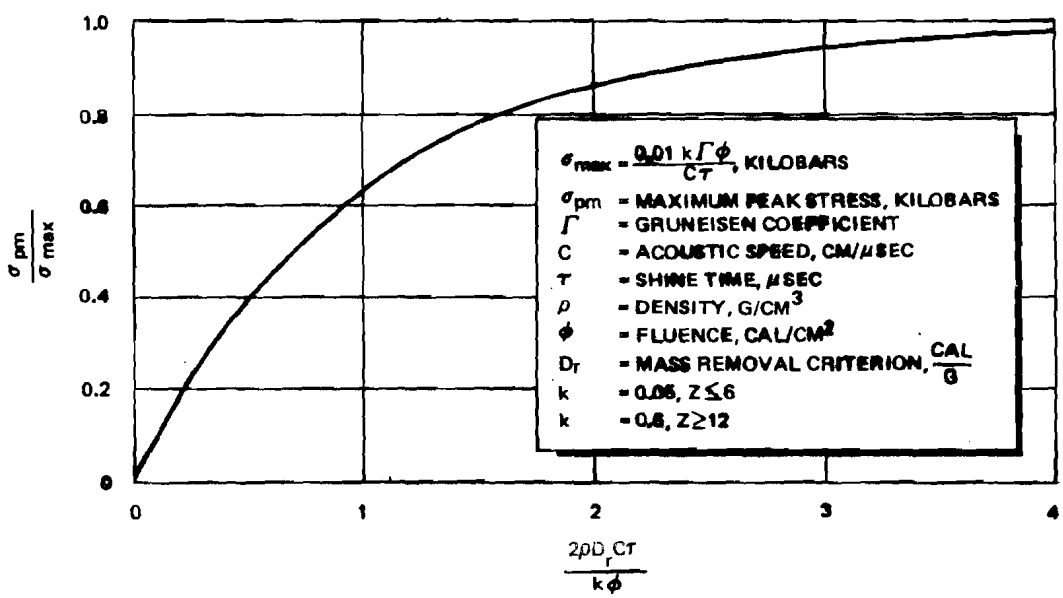

Figure 13. Optimum Thermomechanical Stress

$$T_{op} = 130 \left(\frac{\phi}{D_r}\right)^{2/3} , \qquad Z \geq 40 \tag{80b}$$

As indicated, Equation (80b) agrees well with computer results only for $Z \geq 40$. Figures 3 through 7 can easily be used to estimate T_{op} by setting $D_o/\phi = D_r/\phi$ and estimating the corresponding T by interpolation.

6.2.4 Initial Conditions for Attenuation Analysis

It is recommended that the attenuation of tensile stress amplitude be ignored for the following reasons: (1) there is no adequate theory to handle it, (2) tensile stresses are necessarily below the relatively low spall threshold and thus attenuate weakly with distance, (3) thermomechanical tensile stresses are usually of concern only for structures with relatively small material thicknesses in which attenuation is limited, and (4) ignoring the attenuation that does occur results in conservative estimates.

The attenuation of thermomechanical compressive stresses can be analyzed in the same manner as impulse-induced compressive stresses, as described in Section 7. To do this requires that σ_o and δ_o, the initial peak (equilibrium) compressive stress and the spatial pulse width, be properly specified.

Section 7 defines σ_o and δ_o, with the former defined above and the latter given by

$$\delta_o = \frac{2CI}{\sigma_o} \tag{81}$$

Substituting Equation (71) and Equation (72) with $x = C\tau$ into Equation (81) gives the general expression for δ_o as

$$\delta_o = \frac{2C\tau}{1 - e^{-\frac{2C\tau}{\ell}}} \tag{82}$$

This equation is used in conjunction with Equation (75) (i.e., $\sigma_o = \sigma_p$) as initial conditions for determining stress wave attenuation. It compares

closely with PUFF-type calculations, which might be expected since the compressive stress is almost linear with depth for $0 \leq x \leq C\tau$ and $0 \leq t \leq \tau$ (while the tensile stress is zero for $t \leq \tau$).

For maximum peak stress, Equation (82) becomes

$$\delta_o = 2C\tau \left(1 - e^{-\frac{2\rho D_r C\tau}{k\phi}}\right)^{-1} \tag{83}$$

This equation is used in conjunction with Equation (79).

Equations (82) and (83) differ from Equation (67) by the denominator.

6.3 COMBINED STRESSES

As indicated in Section 5 (See Figure 12), there is a narrow transition between the conditions where no blowoff impulse occurs (thermomechanical stress is dominant) and the conditions approaching maximum blowoff impulse (beyond which impulse-induced stress is dominant). Most practical situations are outside this transition regime. Within this regime, it is considered adequate for design purposes to treat impulse-induced stresses and thermomechanical stresses separately, and to superimpose them. For the two types of concurrent stresses to be consistent, D_r should equal the energy threshold of the particular blowoff impulse model used (i.e., $D_r = E_t$).

6.4 SUMMARY

This section presents analytical relationships that define the initial compressive stress and pulse width associated with blowoff impulse; i.e., Equations (58) and (67). The temporal pulse width τ is equal for most situations to the shine time, for $\phi < 70$ cal/cm^2. Otherwise, it is determined by the gasdynamics and is given by Equation (62), or for optimum conditions, by Equation (66). The initial stress amplitude is attenuated and the pulse width broadened as the stress wave propagates, as discussed in Section 7.

Equations (58) and (67) assume a square stress wave, which corresponds to a constant radiation flux. For the situations where the pulse width is determined by the shine time, the stress spatial and temporal profile follows the flux temporal profile (i.e., it has the same time-dependence). Consequently, if a nonconstant flux profile is known, σ_o can be defined accordingly by applying Equation (72), with Equations (58) and (67) still applicable.

This section also presents analytical relationships for the peak tensile and compressive thermomechanical stresses formed near the surface of an exposed material. Relationships are given for a fixed dose profile and for the optimum dose profile that maximizes the peak equilibrium stress for blackbody spectra.

Tensile stress wave attenuation is disregarded. Compressive stress wave attenuation should be accounted for as described in Section 7; the relationships derived here are used as initial conditions for subsequent compressive stress wave attenuation.

The general relationship for peak (equilibrium) tensile or compressive stress is Equation (74), and the corresponding initial pulse width is Equation (82). In general, it is important to impose the condition of Equation (76). Similar relationships for optimum spectra are Equations (79) and (83), in which the condition of $D_s = D_r$ is incorporated. These equations include the important effect of stress relaxation during a finite shine time. One result of the shine-time effect is that peak thermomechanical stresses are weakly material-dependent, especially for optimum conditions.

Impulse-induced stresses and thermomechanical stresses occur, for the most part, exclusive of each other; that is, either one or the other is almost always clearly dominant. This is definitely the case for all optimum situations. If one wishes to treat them as concurrent but separate, as for a specific blackbody temperature, this can be done straightforwardly by setting D_r equal to the energy threshold of the blowoff model used, and using the appropriate fluence and ℓ for the material not removed by blowoff, as determined from energy deposition curves. The impulse-induced stress would then be determined as has been described.

Section 7
STRESS WAVE ATTENUATION IN UNDISTENDED MATERIALS

The attenuation of the amplitude of a compressive stress wave as it propagates into a structure is one of the main phenomena that must be accounted for in analyzing stress wave effects. Consequently, it has been the subject of considerable experimental and theoretical research that has produced a large body of literature which is heavily oriented toward theory rather than practicality. A brief discussion is provided to put the practical aspects of the subject in perspective.

7.1 BACKGROUND DISCUSSION

There are two basic approaches to analyzing stress wave attenuation. The first one, the one that has received the most attention, involves the use of computer programs such as the PUFF code, which performs sophisticated calculations to account for (1) a detailed description of the equation-of-state, (2) an exact numerical solution of the hydrodynamic equations, (3) time-dependence of imposed loads, (4) temperature-dependence of material properties, (5) nonidealized wave forms, and (6) interference effects, as well as other factors. The second approach is more analytical and is based on the use of so-called weak-shock theory, which accounts for mechanical effects only. The essential difference between the two approaches is that the second uses a simplified equation-of-state involving only the Hugoniot (i.e., a nonlinear, nonelastic, hydrostatic stress-strain relationship). It therefore cannot account for the effects of thermodynamics, porosity, elastic strength, phase changes, strain rate, work hardening, inhomogeneties, etc. Exact solutions of weak-shock theory require a computer code and can therefore include most other aspects of the stress wave problem. However, the real advantage of the second approach is its application to obtain a convenient, explicit, general analytical solution to idealized stress wave problems. This approach makes possible the practical application of stress wave attenuation theory, and greatly promotes physical understanding. Neither of the two approaches can properly treat the attenuation of tensile stress waves.

Although a number of theoretical questions can be raised about the validity of PUFF-type calculations under certain conditions and for certain kinds of materials, they appear generally to agree with experiment. Most uncertainties in results are due to uncertainties in the equation-of-state. In any case, detailed PUFF-type calculations represent the only consistent basis for assessing simpler representations like weak-shock theory.

A number of comparisons of weak-shock theory have been made with PUFF-type calculations for various materials and stress levels, some published (e.g., early work by the developers on the BBAY blowoff model and a 1970 study by Bertholf and Oliver[7]) and some unpublished. General agreement is good for most materials and stress levels relevant to weapon systems. Generally, when the proper initial conditions are used, the results for relatively large thicknesses and initial stresses (i.e., thicknesses greater than approximately 100 times the initial pulse width and initial stresses greater than several hundred kilobars), and for all thicknesses and low initial stresses ($\leq$ 100 kilobars) are approximately the same for the two methods of analysis. For smaller thicknesses and large initial stresses, the deviation is relatively small, around 20 to 30 percent for most comparisons that have been examined. An exception is porous materials, which involve crushing as the dominant attenuation mechanism; they must therefore be treated as a separate class of materials, and are discussed in Section 8.

Thus, for most undistended or fully dense materials, the weak-shock theory is entirely adequate for practical application to the analysis of stress wave effects. Problems that arise from the approximations involved are more often theoretical than practical. Further, a precise knowledge of stress waves is only as useful as the accuracy with which material damage criteria are known. There are virtually no definitive stress-wave damage criteria available for most materials because of the difficulty of measuring such data. Typical criteria that are used for design (not research analysis) do not even explicitly include pulse width as a parameter, and peak stress criteria are often not known to better than a factor of 2 or 3.

---

[7] L.D. Bertholf and M.L. Oliver, Approximate Analytic Expressions for the Attenuation of a Triangular Pressure Pulse with Distance, Sandia Laboratories, SC-RR-69-596, February 1970.

A further general indication of the validity of weak-shock theory for other than very high stresses where thermodynamic effects occur, can also be inferred from the extent to which a linear relationship holds between shock velocity and particle velocity, which is one representation of the Hugoniot. Departures from linearity can usually be traced to porosity, material strength properties associated with a high elastic yield strength, or phase transitions.[7] At typical stresses, phase transitions and thermodynamic effects are not important in most materials. The Hugoniot elastic limit is seldom important because it is operative only at stresses so low that attenuation is too weak to be very significant anyway, at least over typical thicknesses of high-strength materials (e.g., maraged steel). And porosity is treated by a different technique than weak-shock theory, as previously stated. Of the 74 diverse materials included in Kohn[8], a linear relationship is valid for 90 percent of them.

Finally, when an attenuation theory like weak-shock theory is referenced to actual surface conditions at zero thickness, is asymptotically correct or approximately correct at large thicknesses, and has the correct fundamental behavior, it is difficult for it to be in serious error if used correctly.

Therefore, weak-shock theory in general and the following general equation derived from it in particular can usually be used with the same confidence, from a practical standpoint, as PUFF-type analyses for all but a few materials. It is recommended for general use.

7.2 ASYMPTOTIC WEAK-SHOCK THEORY

Weak-shock theory, as applied to x-ray effects was developed by W. L. Bade et al. for the Air Force Special Weapons Center circa 1962. This representation involved numerical analysis, and was not applicable to small thicknesses because the initial (surface loading) conditions involved only the impulse rather than the initial stress and pulse width being imposed independently. Other derivations (e.g., Bertholf and Oliver[7]) treat the initial conditions explicitly, but also have the disadvantage of requiring numerical analysis.

---

[7] Ibid.

[8] Brian J. Kohn, Compilation of Hugoniot Equations of State, Air Force Weapons Laboratory, AFWL-TR-69-38, April 1969.

The following derivation differs from that of Bertholf and Oliver[7] in that the asymptotic approximation of weak-shock theory is used here; that is, only first-order terms are retained in the relationship between stress and wave velocity. This approximation allows an explicit analytical expression to be obtained for stress as a function of propagation distance, and it gives good agreement with PUFF-type calculations.

One way of visualizing stress wave attenuation is that the front of the wave, or the loading wave, travels at a higher velocity than the rear of the wave, or unloading wave. This spreads the stress wave with time or propagation distance. Since the area (impulse) of the stress wave must remain constant to conserve momentum and if the shape of the stress wave remains constant, then the peak pressure will be inversely proportional to the pulse width. Any initial stress wave quickly degenerates into an approximately triangular pulse shape, with the peak stress corresponding to an almost vertical shock front and the stress decreasing linearly to approximately zero at the rear of the wave. Bertholf and Oliver[7] show that deviations from an idealized triangular stress wave have no significant effect on peak stress attenuation.

For convenience, the S-Hugoniot mentioned earlier will be used. It has the form

$$U = C + Su \tag{84}$$

where U is the shock velocity, C is the acoustic velocity at zero stress, S is the Hugoniot slope for a given material, and u is the particle velocity. Relative to undisturbed material, the stress wave moves with velocity $C_s + u$, with C_s given by

$$C_s^2 = \frac{\partial \sigma}{\partial \rho} \tag{85}$$

where C_s is the acoustic velocity at finite stress σ and density ρ_s. The application of the conservation of mass and momentum to Equation (84) gives the stress as a function of density[7] as

[7] Op. cit.

$$\sigma = \frac{K\alpha}{(1-S\alpha)^2} \tag{86}$$

where K is the bulk modulus ($K = \rho C^2 = E/3(1-2\nu)$, with E Young's modulus and ν Poisson's ratio), and α is defined as

$$\alpha = 1 - \frac{\rho}{\rho_s} \tag{87}$$

where ρ is the density at zero stress. Using Equations (85) and (86),

$$\frac{C_s}{C} = \frac{(1-\alpha)\,(1-S^2\alpha^2)}{(1-S\alpha)^2}^{1/2} \tag{88}$$

Expanding Equation (88) and retaining only terms linear in α gives

$$\frac{C_s}{C} \simeq 1 + (2S-1)\alpha \tag{89}$$

Conservation of mass and momentum give for u[7],

$$u^2 = \sigma\alpha/\rho \tag{90}$$

From Equation (86),

$$\alpha = \frac{\sigma}{K} \tag{91}$$

so that combining Equations (90) and (91) gives

$$u \simeq C \left(\frac{\sigma}{K}\right) \tag{92}$$

and combining Equations (89) and (91) gives

---

[7] Bertholf and Oliver, op. cit.

$$C_s \simeq C + C\,(2S-1)\,\frac{\sigma}{K} \tag{93}$$

Equations (92) and (93) represent asymptotic weak-shock theory.

7.3 DERIVATION OF ATTENUATION EQUATION

The front of the equilibrium (triangular) stress wave moves with velocity $C_s + u$, where C_s and u are defined by the peak stress. The rear of the stress wave moves with velocity $C_s + u \simeq C$, at approximately zero stress. Therefore, the stress wave broadens with time t and distance x as

$$\Delta\delta = (C_s + u - C)\,t = 2S\sigma Ct/K = 2S\sigma x/K \tag{94}$$

where δ is the pulse width, $\Delta\delta$ is the increase in δ in distance x, and $x = Ct$. To conserve momentum,

$$\sigma\delta = \sigma_o \delta_o = 2IC \tag{95}$$

where σ_o is the initial peak stress, δ_o is the initial (triangular) pulse width, and I is the impulse load. For $x \gg \delta_o$, $\delta \simeq \Delta\delta$ so that Equations (94) and (95) give

$$\sigma = \left(\frac{\sigma_o \delta_o K}{2Sx}\right)^{1/2} = \left(\frac{ICK}{Sx}\right)^{1/2} \tag{96}$$

for large x. Using Equation (96), an effective finite thickness x_o is assigned to the surface to introduce the initial stress condition:

$$x_o = \frac{\delta_o K}{2S\sigma_o} \tag{97}$$

and x is replaced in Equation (96) by $x + x_o$ to give

$$\frac{\sigma}{\sigma_o} = \left[1 + 2S\left(\frac{\sigma_o}{K}\right)\left(\frac{x}{\delta_o}\right)\right]^{-1/2} \tag{98}$$

This is the stress wave attenuation relationship obtained from asymptotic theory. The same result is obtained with a more rigorous and longer derivation.

Equation (98) is for a single material. It is easily extended to handle a laminated structure by following the above procedure and assigning a new x_o at each material boundary. The result after algebraic simplification, is

$$\frac{\sigma}{\sigma_o} = T_t\left[1 + \frac{2\sigma_o}{\delta_o}\sum_i \frac{S_i\, x_i}{K_i}\right]^{-1/2} \tag{99}$$

where the indicated sum is over all material thicknesses from the surface to the depth at which the stress is evaluated, and T_t is the product of the individual acoustic transmission factors for all intervening material boundaries. T_t is defined by

$$T_t = \prod_i T_i \tag{100}$$

and

$$T_i = 2\left[1 + \frac{(\rho C)_i}{(\rho C)_{i+1}}\right]^{-1} \tag{101}$$

where T_i is for the i^{th} boundary formed by laminates i and i+1.

The pulse width is given by Equation (95):

$$\frac{\delta}{\delta_o} = \frac{\sigma_o}{\sigma} \tag{102}$$

Table 3 gives a compilation of S values or Hugoniot slopes taken from Kohn[8]. They do not vary much with material, as is the case with the Gruneisen coefficient Γ, because theoretically $\Gamma = 2S-1$ (e.g., Glover[9]), which appears in Equation (93).

7.4 COMPARISON WITH PUFF-TYPE RESULTS

Figure 14 shows, for aluminum, a comparison between asymptotic weak-shock theory as represented by Equation (98), full weak-shock theory, and a PUFF-type calculation made with the WONDY code[10]. The last two curves were taken from Bertholf and Oliver[7]. The comparison is excellent for all thicknesses at 50 kilobars, with Equation (98) giving, in this case, the same result as WONDY. The comparison is good for all thicknesses at 250 kilobars, with Equation (98) being approximately 25 percent lower than the WONDY result for $2 \leq x/\delta_o \leq 100$, and approaching the WONDY result for other distance ratios. Results for 1,000 kilobars are shown only as a matter of interest, since stresses this high are of practical significance only when large thicknesses are involved (and for which δ_o is typically of the order of 10^{-2} cm). Even at this high initial stress level, Equation (98) is within 25 percent of WONDY for $x/\delta_o \geq 100$, but falls to about 50 percent of WONDY for smaller thicknesses. Even the latter comparison is comparable to uncertainties in failure criteria.

---

[7] Op. cit.

[8] Op. cit.

[9] J.E. Glover, Dynamic Measurements of the Gruneisen Coefficients of Tantalum, Uranium, and Uranium-Molybdenum Alloys, Sandia Laboratories SC-RR-71-0314, August 1971.

[10] W. Herrmann and P. Holzhauser, WONDY, A Computer Program for Calculating Problems of Motion in One Dimension, Sandia Laboratories, SC-RR-66-601, February 1967.

Table 3

HUGONIOT SLOPES

Material	S	Material	S	Material	S
Aluminum	1.33	Gold	1.50	X-cut Crystalline quartz	N/A*
Aluminum (1060)	1.44	Graphite commercial	N/A*	Phenolic refrasil	1.01
Aluminum (6061-T6)	N/A*	Pyrolytic graphite	1.73	Platinum	1.54
24ST Aluminum	1.34	Hafnium	1.12	Plexiglas	1.45
921 T Aluminum	1.42	Armco Iron	3.14	Polyethylene	1.47
Aluminum (2024)	1.37	Lead	1.45	Polystyrene	1.20
Antimony	1.54	Lucite	1.83	Polyurethane	N/A*
Avcoat II	1.68	Magnesium	1.24	RAD 58B	0.68
Beryllium	1.14	Manganin	1.72	OTWR	N/A*
Bismuth	1.93	Molybdenum	1.24	Series 124 resin	1.89
Boron nitride	2.73	Mylar	1.63	Silver	1.54
Brass	1.43	Nickel	1.45	Stainless Steel Type 304	1.51
Cadmium	1.66	Niobium	1.21	Stainless Steel Type 304L	1.49
Boron carbide	1.81	Nylon	1.55	Steel, mild EN3	1.69
Silicon carbide	1.66	Palladium	2.00	Tantalum	1.32
Tungsten carbide	1.16	Paraffin	1.53	Teflon	1.97
Carbon phenolic	N/A*	AVCO Phenolic fiber glass	1.17	Thallium	1.50
3-D Carbon phenolic	1.43	GE Phenolic fiber glass	1.05	Thorium	1.25
Chromium	1.38	Chopped nylon phenolic	1.61	Tin	1.52
Cobalt	1.30	Tape-wound nylon phenolic	1.32	Titanium	1.15
Copper	1.49	Quartz phenolic	1.03	Tungsten	1.30
Durite	1.41	3-D Quartz phenolic	0.96	TWSP	1.08
Epoxy	1.52	Zirconium	1.02	Uranium-3 wt pct Molybdenum	1.53
C-7 Epoxy	1.44			Vanadium	1.20
Zinc	1.55				
Exon	1.66				
Hi-D Glass	N/A*				

*The linear relationship of Equation (84) does not hold.

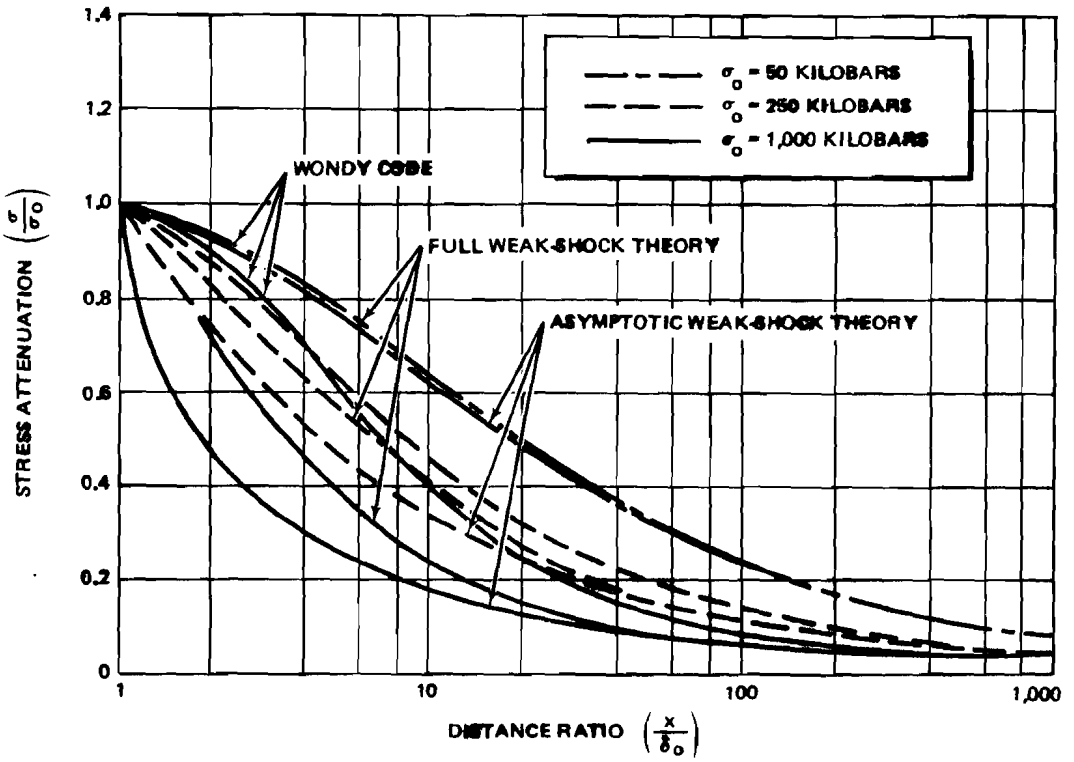

Figure 14. Comparison of Stress Attenuation for Aluminum

7.5 SUMMARY

Based on the reasons and comparison given above, and on other similar comparisons with theory and a few experiments, Equations (98) through (102) are recommended for general use. It is expected that PUFF-type analyses would be required only for occasional verification and for unusual or very specific problems.

The equations are applicable to compressive stresses due either to impulse loads or to thermomechanical stresses. The definition of the initial conditions are discussed in Section 6. In all cases, the initial stress wave is assumed to be triangular. The actual initial stress wave will relax to the equilibrium triangular shape within approximately the time it takes for the differential velocity between the loading wave and the unloading wave to propagate a distance equal to the initial pulse width. For example, for an initial square wave of width δ_o, use of Equation (94) shows that the distance required for the pulse to become approximately triangular is x_o, given by Equation (97).

Tensile stress propagation cannot be analyzed as rigorously as compressive stress propagation. Because tensile stresses are necessarily limited to amplitudes less than the fracture threshold and because the attenuation at these levels is therefore relatively weak, it is recommended that attenuation of tensile stresses be ignored for practical analysis. This will tend to give conservative estimates.

The equations as they stand apply only to first-pass or single-transit stresses, which are dominant for most situations. However, the equations can be straightforwardly applied to estimate reinforcement due to stress wave reduction. This is relatively easy for first-order reflections, but soon becomes tedious for multiple reflections.

Section 8

STRESS WAVE ATTENUATION IN DISTENDED MATERIALS

One of the methods for reducing blowoff-induced stress wave damage is to provide a porous or foam (i.e., distended) material that attenuates the stress wave amplitude to a tolerable level. The dominant attenuation mechanism in porous materials is the spreading of the pulse width caused by their large compressibility, which is far more effective than the mechanical hysteresis mechanism of undistended materials.

Aside from the inconvenience and cost of a PUFF-type analysis of stress wave attenuation, a paucity of experimental data on the equation-of-state of porous materials poses a difficulty. Therefore, an analytical relationship that does not require an explicit definition of the equation-of-state is highly desirable. Such a relationship is obtained using the phenomonological snowplow model (e.g., Herrmann[11]).

8.1 THE SNOWPLOW MODEL

The snowplow model assumes that the only stress wave attenuation mechanism is due to the compaction of the porous material. It assumes that the porous material is compacted to its solid density and that no energy is absorbed by the crushing action, but that all energy from the imposed impulse load goes into the formation of a stress wave uniformly distributed in the solid (compacted) material. The yield or crush strength is assumed to be negligible compared to the applied pressure. Thus, as the pressure pulse encompasses more compacted material, it broadens and the amplitude decreases. Since basically only the conservation of energy and momentum is involved, the model requires no explicit knowledge of the material equation-of-state.

---

[11] W. Herrmann, Constitutive Equations for the Dynamic Compaction of Ductile Porous Materials, J. Applied Phys., Vol. 40, No. 6., pp 2490-2499, May 1969.

If the material, as it is compacted at a pressure p, is uniformly stressed to the same pressure, the compacted material represents a square stress wave with a spatial pulse width equal to the thickness of compacted material, and the impulse is equal to the imposed impulse load. With a uniform compacting pressure equal to the stress in the compacted material, the compaction energy expended is equal to the energy in the stressed solid material, the latter being the sum of the kinetic energy and the stored strain-energy. Therefore,

$$pxf_v = \frac{\rho(1-f_v)xu^2}{2} + \frac{K}{2}\epsilon^2 x(1-f_v) = mu^2 \qquad (103)$$

where p is the compacting pressure acting over distance xf_v, with x the front of the stress wave as measured from the original surface, and f_v the porosity or void fraction. The mass of solid material which the pressure pulse encompasses is $m = \rho(1-f_v)\,x$, where ρ is the density of the solid material, u is the particle velocity, K is the bulk modulus of the solid material, and ϵ is the unit strain of the solid material. The first term on the right side of Equation (103) is the kinetic energy and the second term is the strain energy. The strain energy is equal to the kinetic energy for a linear-elastic material. Since the stress σ is equal to the pressure and the impulse $I = mu$, Equation (103) becomes

$$\sigma = \frac{10^{-3}}{\rho f_v (1-f_v)} \left(\frac{I}{x}\right)^2 \qquad (104)$$

which gives the stress in kilobars at depth x cm, for a porous material of porosity f_v and solid density ρ g/cm^3, and an impulse of I kilotaps. This is the stress as a function of I and x as given by the snowplow model.

8.2 STRESS WAVE ATTENUATOR SIZING

The required thickness of a stress wave attenuator material is usually determined by the stress amplitude transmitted into the underlying structural material. Rearranging Equation (104) and letting h represent the porous attenuator thickness in cm,

$$h = 0.045I \left[\sigma_c \rho f_v (1-f_v) \left(1 + \frac{(\rho C)_s}{(\rho C)_a} \right) \right]^{-1/2} \qquad (105)$$

where the units are as for Equation (104), σ_c is the allowable stress criterion for the structural material, ρC is the acoustic impedance, C is the acoustic velocity, and the subscripts a and s refer to the properties of the solid attenuator material and the underlying structure, respectively. Equation (105) includes the stress wave transmission factor T_t which relates the stress at the rear of the attenuator, σ_a, to the stress transmitted into the adjacent structure, σ_s, where

$$T_t = \frac{\sigma_s}{\sigma_a} = \frac{2}{1 + \frac{(\rho C)_s}{(\rho C)_a}} \qquad (106)$$

The most desirable void fraction is that corresponding to the least mass of attenuator material required to achieve a given stress reduction. Although no finite optimum f_v is indicated by the snowplow model, more detailed computer analyses indicate that it is approximately 0.5 for all materials.

8.3 SUMMARY

The snowplow model, as represented by Equations (104) and (105), has been compared with experiment and with more elaborate analyses (e.g., Herrmann[11]), and shown to be qualitatively correct and reasonably accurate. For transmitted stresses greater than approximately 10 kilobars, it predicts for a given attenuator thickness stresses that are usually high by less than a factor of 2, with generally greater accuracy for higher stresses. For low stresses of a few kilobars, it tends to predict stresses that are high by approximately a factor of 2. This corresponds to predicting, for a given stress, thicknesses that are high by 40 percent. It is therefore somewhat conservative, but adequate for preliminary sizing; more detailed calculations are desirable for final design only if an adequate equation-of-state is available.

[11] Ibid.

Section 9
STRUCTURAL RESPONSE

Structural response refers here to the dynamic circumferential motion of a structure responding to a rapidly applied transient load, usually resulting from blowoff impulse. It has potential importance only for large, relatively fragile structures. Thermomechanical pressure pulses due to x-ray heating of liquids and their containers can also cause structural response.

Deformation associated with structural response can in principle cause debonding, buckling, or rupture. Solid propellant damage is not considered a problem because of the case-limited strain and deflection of typical high-stiffness case materials. However, in reality it is seldom a critical damage mode because either the loads of interest are too small or material response damage modes are more critical. Material response is usually critical; however, liquid tanks can be damaged by shock pressures induced by relatively low fluences.

Impulsive loads are those whose duration is short compared to typical structural response times (0.1 to 1 msec). They are induced by blowoff impulse or pressure pulses induced in liquids. An equivalent impulse load can be caused by a thermal load due to rapid thermal expansion in the circumferential and consequently the radial directions. However, for a given fluence, blowoff impulse loads will usually be more critical.

This section summarizes analytical relationships suitable for general analysis. They are not derived here, but are taken from Langley[12].

---

[12] R.W. Langley, Structural Response of Propulsion Systems, McDonnell Douglas Paper No. WD 2357. Presented at the Fourth Symposium on Nuclear Survivability of Propulsion and Ordnance Systems, April 1974.

9.1 SHELL BUCKLING OR RUPTURE

The general equation that defines the critical impulse to cause shell failure is

$$I_c = \frac{h}{C} F_m \left[2E \int_{\epsilon_{st}}^{\epsilon_c} \sigma(\epsilon)\, d\epsilon \right]^{1/2} \tag{107}$$

where I_c is the critical impulse in kilotaps, h is the load-carrying shell thickness in cm, C is its acoustic velocity in cm/μsec, E is Young's modulus in kilobars, ϵ is the dimensionless strain, ϵ_c is the strain criterion at which failure occurs, ϵ_{st} is the strain corresponding to any static stress that may exist, and $\sigma(\epsilon)$ is the (engineering) stress of the material in kilobars as a function of strain (i.e., the conventional stress-strain curve). For buckling, ϵ_c corresponds to the strain-to-yield stress and for rupture it corresponds to the strain-to-ultimate stress. For a linear stress-strain curve, the term in brackets becomes $(\sigma_c - \sigma_{st})$, where the subscripts correspond to those for the strains in the equation.

The factor F_m accounts for a multishell structure, and is given by

$$F_m = \left[\left(1 + \frac{\rho_2 h_2}{\rho_1 h_1} + \frac{\rho_3 h_3}{\rho_1 h_1} + \ldots \right) \left(1 + \frac{E_2 h_2}{E_1 h_1} + \frac{E_3 h_3}{E_1 h_1} + \ldots \right) \right]^{1/2} \tag{108}$$

where ρ is density, subscript 1 refers to the shell whose response is being analyzed, and the other subscripts refer to other laminates making up the multishell structure. Equation (108) shows that the response is greatest (I_c is smallest) when the mass of the structure is smallest.

Because a liquid cannot transmit a significant tensile stress, liquid tankage can be damaged by the positive half of the momentum introduced by absorbed x-rays, even if no net impulse is created by blowoff. In this case, the

critical impulse is given by Equation (107), but the impulse is related to the fluence by [see Equation (71)]

$$I = 0.021\phi \left[\frac{\Gamma_t}{C_t} f + \frac{\Gamma_\ell}{C_\ell} (1 - f)\right] \tag{109}$$

where I is in kilotaps, ϕ is in cal/cm^2, Γ is the Gruneisen coefficient, subscript t refers to the tank material, subscript ℓ refers to the liquid, and f is the fraction of the incident fluence absorbed by the tank wall (but does not contribute to front-face mass removal). If blowoff impulse occurs, it will cancel all or part of the impulse of Equation (109) because the two types of impulse are oppositely directed.

9.2 DEBONDING

Debonding by structural response is very unlikely, even for large fluences; material response damage is usually far more critical. The equation for estimating the critical impulse at which debonding will occur in a two-material bonded structure is

$$I_c = \frac{\sigma_c G(\omega)}{\Delta\omega} \tag{110}$$

where I_c is in kilotaps, σ_c is the dynamic bond strength or debond criterion in kilobars, and $\Delta\omega$ is the beat frequency defined as

$$\Delta\omega = \left|\omega_1 - \omega_2\right| \tag{111}$$

with the vibrational frequency of the two structural materials, designated by the subscripts, given by

$$\omega = \frac{C}{\Gamma} \tag{112}$$

Where ω is in μsec^{-1} and R is the radius of the cylindrical structure in cm.

$G(\omega)$ is given by

$$G(\omega) = \frac{(1 + a)^{3/2} \left(1 + a \frac{\omega_2^2}{\omega_1^2}\right)^{1/2}}{a \left(1 + \frac{\omega_2}{\omega_1}\right)} \tag{113}$$

where a is defined as

$$a = \frac{\rho_2 h_2}{\rho_1 h_1} \tag{114}$$

The minimum of Equation (110) is

$$I_{c_{min}} = \frac{2\sigma_c}{\Delta\omega} \tag{115}$$

and occurs at a = 1. This indicates that the critical impulse is smallest when the masses of the two materials are approximately equal, although the exact value of the optimum value of a depends on ω_1/ω_2 as indicated by Equation (113).

Section 10
DESIGN EQUATIONS

This section combines some of the relationships derived previously to obtain equations in terms of explicit expressions for fluence thresholds for specific failure mechanisms and typical structural configurations. Some equations for dose and peak stress are also summarized. Other expressions can be similarly obtained. All the threshold expressions are for optimum spectra, corresponding to minimum fluence thresholds. The equations are all for normally incident radiation: Section 10.16 explains how oblique incidence is handled. All Z's refer to effective atomic numbers.

If the optimum blackbody temperature for a given effect is outside the range of specified temperatures, then the threshold for the appropriate limiting blackbody temperature must be determined. For specific blackbody temperatures, explicit expressions for fluence thresholds are generally not possible. However, the equations, figures, and explanations given in this report can easily be used to generate plots of fluence thresholds versus the values of failure criteria, and the thresholds for specific criteria and blackbody spectra can thus be obtained.

The symbols and units are the same as defined for the identified constituent equations that are combined to obtain a given expression. The design equations, which are listed in the table of contents, are summarized in Tables 4 and 5. The units used are calories, grams, centimeters, microseconds, kilobars, kilotaps, and kev; all fluence thresholds are in cal/cm^2.

10.1 MAXIMUM DOSE IN A SUBSURFACE MATERIAL

Equation (9) gives directly the fluence threshold for the maximum dose in a subsurface material:

$$\phi_t = \frac{D_c}{a} (\rho x)^b \, (Z_s^n / Z_a^n) \tag{116}$$

where D_c is the specified dose criterion, and the parameters a, b, and n are given in Table 2. The quantity ρx is the total material areal density in g/cm^2 up to the front face of the subsurface material being considered, and Z_s and Z_a are defined by Equation (10).

The optimum blackbody temperature is given by Equation (23) or (24), depending on the value of b.

10.2 MAXIMUM FRONT-FACE MASS REMOVAL

The fluence threshold for maximum mass removal is given directly by Equation (25):

$$\phi_t = 4.2 \, \rho D_r x_c \tag{117}$$

where x_c is the specified threshold criterion. The optimum blackbody temperature is given by Equation (23).

10.3 STRUCTURAL HEATING FOR OPTIMUM CONDITIONS

The fluence threshold for a specified bulk temperature rise can be obtained from Equation (35) for optimum conditions. However, because this equation is transcendental in ϕ, the fluence threshold can be most conveniently obtained from Figure 11 by a trial-and-error procedure. The optimum blackbody temperature is given by Equation (37).

10.4 PEAK COMPRESSIVE STRESS IN A SUBSURFACE MATERIAL DUE TO MAXIMUM BLOWOFF IMPULSE

The general equation for maximum blowoff impulse is, from Figure 12,

$$I_{max} = \frac{A\phi}{E_t^{1/2}} \tag{118}$$

Combining Equations (59), (67), (99), and (118) gives the peak compressive stress in a subsurface material due to maximum blowoff impulse:

$$\sigma_p = \frac{A\phi T_t}{\tau E_t^{1/2}} \left(1 + \frac{A\phi \Sigma_i}{C\tau^2 E_t^{1/2}} \right)^{-1/2} \tag{119}$$

where T_t is the overall transmission coefficient defined by Equations (100) and (101), and includes all boundaries up to the material in which the stress is evaluated. The symbol Σ_i indicates the following summation of paramters in Equation (99):

$$\Sigma_i = \sum_i \frac{S_i x_i}{K_i} \tag{120}$$

The summation is up to the point at which the stress is evaluated.

The optimum blackbody temperature is given by Equation (51) or (52), depending on the blowoff model used.

10.5 BACK-FACE SPALL OF A SURFACE MATERIAL DUE TO MAXIMUM BLOWOFF IMPULSE

Rearranging Equation (98) gives

$$\sigma_o^2 - \left(\frac{2Sx\sigma^2}{K\delta_o} \right) \sigma_o - \sigma^2 = 0 \tag{121}$$

where σ is the compressive stress at the back face of the surface material. Setting the reflected tensile stress σ_r to the spall criterion σ_s,

$$\sigma_r = \sigma T_r = \sigma_s \tag{122}$$

where T_r is the reflection coefficient between the surface material and any contiguous subsurface material, and is given by

$$T_r = \frac{(\rho C)_2 - (\rho C)_1}{(\rho C)_1 + (\rho C)_2} \tag{123}$$

Subscript 1 refers to the surface material, subscript 2 to the subsurface material, and ρC is the acoustic impedance. If there is no subsurface material, $T_r = -1$. If $T_r < 0$, this indicates a reflected stress wave that changes from compressive to tensile, or vice versa.

Solving Equation (121) for σ_o, and substituting for σ from Equation (122) and for δ_o from Equation (67), σ_o is given by

$$\sigma_o = \frac{Sx\sigma_s^{\,2}}{2C\tau KT_r^{\,2}} \left\{ 1 + \left[1 + \left(\frac{2C\tau KT_r}{Sx\,\sigma_s} \right)^2 \right]^{1/2} \right\} \tag{124}$$

Combining Equations (59), (118), and (124) gives ϕ_t for causing back-face spall of a surface material due to maximum blowoff impulse;

$$\phi_t = \frac{Sx\sigma_s^{\,2} E_t^{\,1/2}}{2ACKT_r^{\,2}} \left\{ 1 + \left[1 + \left(\frac{2C\tau KT_r}{Sx\sigma_s} \right)^2 \right]^{1/2} \right\} \tag{125}$$

The optimum blackbody temperature is given by Equation (51) or (52), depending on the blowoff model used.

10.6 BACK-FACE SPALL OF A SUBSURFACE MATERIAL DUE TO MAXIMUM BLOWOFF IMPULSE

Equation (99) generalizes Equation (98) by letting

$$\sigma \rightarrow \frac{\sigma}{T_t} \tag{126}$$

and

$$\frac{Sx}{K} \rightarrow \Sigma_i \tag{127}$$

where Σ_i is defined by Equation (120) and T_t is the overall translation coefficient defined by Equations (100) and (101). Similarly, Equation (125) is generalized to give ϕ_t for causing back-face spall of a subsurface material due to maximum blowoff impulse:

$$\phi_t = \frac{\sigma_s^2 E_t^{1/2} \Sigma_i}{2ACT_t^2 T_r^2} \left\{ 1 + \left[1 + \left(\frac{2C_\tau T_t T_r}{\Sigma_i \sigma_s} \right)^2 \right]^{1/2} \right\} \tag{128}$$

where T_t includes all boundaries up to the material in which the stress is being evaluated; if it is the last material, $T_r = -1$. T_r is defined by Equation (123). Σ_i is summed up to the stress plane of interest.

The optimum blackbody temperature is given by Equation (51) or (52), depending on the blowoff model used.

10.7 BACK-FACE SPALL OF A SURFACE MATERIAL DUE TO MAXIMUM THERMOMECHANICAL STRESS

The maximum tensile stress at the back face is equal to the sum of the reflected, attenuated compressive stress and the unreflected, unattenuated tensile stress. The former is given by Equation (98) multiplied by the reflection coefficient between the surface material and any contiguous subsurface material, with the σ_o of Equation (98) equal to the σ_{pm} of Equation (79) and with δ_o defined by Equation (83). The latter stress is just equal to σ_o or σ_{pm} of Equation (79). Using these three equations to combine the tensile and reflected compressive stresses gives the maximum peak tensile stress at the back face:

$$\sigma_t = \frac{0.01k\Gamma\phi\alpha}{C_\tau} \left[1 - T_r \left(1 + \frac{0.01Sk\Gamma\phi x\alpha^2}{C^2 \tau^2 K} \right)^{-1/2} \right] \tag{129}$$

where T_r is defined by Equation (123) with its sign retained, and α is defined by

$$\alpha = 1 - \exp\left(-\frac{2\rho D_r C\tau}{k\phi}\right) \tag{130}$$

The fluence threshold for spall is obtained by plotting σ_t versus ϕ to determine the $\phi = \phi_t$ corresponding to $\sigma_t = \sigma_s$, where ϕ_t is the fluence threshold and σ_s is the spall criterion. If there is no subsurface material, $T_r = -1$.

For spall to occur at the back face rather than near the front face, the amplitude of the tensile stress, σ_o, must be less than σ_s. If no significant attenuation of the compressive stress occurs and $T_r = -1$, the upper limit of the amplitude of the reflected compressive stress at the back face is also σ_o. Therefore, Equation (129) is valid only for $\sigma_s < \sigma_t < 2\sigma_s$ and is consequently of limited importance relative to back-face spall from maximum blowoff impulse. Nevertheless, it is presented here for the sake of comparison with other spall thresholds.

The optimum blackbody temperature can be obtained from Equation (80) or from Figures 2 through 7, depending on the effective atomic number.

10.8 PEAK COMPRESSIVE STRESS IN A NONCONTIGUOUS SUBSURFACE MATERIAL DUE TO MAXIMUM THERMOMECHANICAL STRESS

The situation analyzed here is for a shielded (subsurface) material in which the thermomechanical stress is generated. The shielded material is noncontiguous with the shielding material (e.g., a component within a shroud). The subsurface materials can generally form a laminated structure with the first material being the material in which the stress is generated.

It is assumed that: (1) there is no front-face mass removed from the shielded material, and (2) the maximum peak stress corresponds to the maximum surface dose in the shielded material. The first assumption will virtually always be true for realistic conditions, and the second assumption is a good approximation for all realistic conditions.

The peak equilibrium stress is given by Equation (75). The surface dose D_s is, by assumption (1), equal to D_o of Equation (76). The maximum dose D_m is therefore given by Equation (53) (for b of Table 2 equal to 1), and the corresponding ℓ_a for the shielded absorber material is given by Equation (56). Equation (53) can be used to verify that $D_o < D_r$. Combining Equation (75) with Equations (53), (55), and (56) gives the peak equilibrium (tensile or compressive) stress generated in the shielded material:

$$\sigma_p = \sigma_o = 2.4 \times 10^{-3} \frac{\Gamma\phi}{C\tau} \left\{ 1 - \exp\left[-\frac{2\rho_a C\tau}{\rho_s x_s} \left(Z_a^{3.3} / Z_s^{3.3} \right) \right] \right\} ,$$

$$b = 1 \qquad (131a)$$

where the appropriate value of n = 3.3 has been shown for b = 1. A similar derivation gives, for b = 3/2,

$$\sigma_o = \frac{2.7 \times 10^{-3} \Gamma\phi}{C\tau(\rho_s x_s)^{1/2}} \left\{ 1 - \exp\left[-\frac{3\rho_a C\tau}{\rho_s x_s} \left(Z_a^{2.8} / Z_s^{2.8} \right) \right] \right\} ,$$

$$b = 3/2 \qquad (131b)$$

and, in general,

$$\sigma_o = \frac{0.01 a \Gamma\phi\beta}{bC\tau(\rho_s x_s)^{b-1}} \qquad (132)$$

where β is defined as

$$\beta = 1 - \exp\left[-\frac{2b\rho_a C\tau}{\rho_s x_s} \left(Z_a^n / Z_s^n \right) \right] \qquad (133)$$

and the general relationship between ℓ_s and x_s has been used:

$$\ell_s = - (d\ell n\, D_m/dx)^{-1} = \frac{x_s}{b} \tag{134}$$

The pulse width corresponding to the σ_o of Equation (132) is given by Equations (82) and (133):

$$\sigma_o = \frac{2C\tau}{\beta} \tag{135}$$

Substituting Equations (132) and (135) into Equation (99) gives, for a specific fluence, the maximum peak compressive stress in a generally laminated shielded structure due to the (approximately) maximum thermomechanical stress formed in the first shielded material, which is noncontigous with the shielded material:

$$\sigma_m = \frac{0.01a\Gamma T_t \phi\beta}{bC\tau(\rho_s x_s)^{b-1}} \left[1 + \frac{0.01a\Gamma\Sigma_i \phi\beta^2}{bC^2\tau^2(\rho_s x_s)^{b-1}} \right]^{-1/2} \tag{136}$$

where $\rho_s x_s$ is the only shielding material parameter involved, T_t is the overall transmission coefficient defined by Equations (100) and (101), and Σ_i is defined by Equation (120). T_t and Σ_i include all boundaries and thicknesses up to the stress plane.

The optimum blackbody temperature is given by Equation (23) or (24), depending on the value of b.

10.9 DEBONDING OF A COMPOSITE/BOND/METAL STRUCTURE DUE TO MAXIMUM BLOWOFF IMPULSE

The tensile stress for this damage mode is due to the compressive blowoff stress generated in the composite material, transmitted and attenuated through the composite/bond/metal structure, reflected at the free metal

surface as a tensile wave, and transmitted without attenuation back through the metal and into the bond.

Equation (128) is modified to provide the debonding threshold for a composite/bond/metal configuration by setting $T_r = -1$ and $T_t = T_{12} T_{23} T_{32}$, where T_{12} is the transmission coefficient between the composite material and the bond, T_{23} is the coefficient between the bond and the metal substructure, and T_{32} (for the reflected tensile wave) is the coefficient between the metal substructure and the bond. In general, Equation (101) indicates that

$$T_{mn} = 2\left[1 + \frac{(\rho C)_m}{(\rho C)_n}\right]^{-1} \tag{137}$$

Thus, ϕ_t is given by

$$\phi_t = \frac{\sigma_c^{\,2} E_t^{\,1/2} \Sigma_i}{2ACT_t^{\,2}} \left\{1 + \left[1 + \left(\frac{2C\tau T_t}{\Sigma_i \sigma_c}\right)^2\right]^{1/2}\right\} \tag{138}$$

where σ_c is the debonding criterion, C and E_t are for the composite material, and Σ_i is, from Equation (120),

$$\Sigma_i = \frac{S_1 x_1}{K_1} + \frac{S_2 x_2}{K_2} + \frac{S_3 x_3}{K_3} \tag{139}$$

The optimum blackbody temperature is given by Equation (51) or (52), depending on the blowoff model used.

10.10 DEBONDING OF A COMPOSITE/BOND/METAL STRUCTURE DUE TO MAXIMUM THERMOMECHANICAL STRESS GENERATED IN THE METAL

The expression derived here is for a situation similar to that considered in Section 10.8, since the stress is generated in the relatively higher-atomic-number subsurface metal, and the shielding material is the composite and

the bond. Because the materials are all contiguous, the assumption of Section 10.8 regarding no front-face mass removal is not relevant.

The compressive stress generated in the metal is transmitted and attenuated through the metal, reflected at the free surface, and transmitted without attenuation back through the metal into the bond. Equation (136) is solved for ϕ in terms of σ; T_t is set equal to T_{32}, where T_{32} (for the reflected tensile wave) is the transmission coefficient between the metal substructure and the bond. In this case, $\Sigma_i = S_3x_3/K_3$ and $\rho_s x_s = \rho_1 x_1 + \rho_2 x_2$, where subscripts 1, 2, and 3 refer to the composite, bond, and metal, respectively. Thus, ϕ_t is given by

$$\phi_t = \frac{48bS_3x_3(\rho_1x_1 + \rho_2x_2)^{b-1}\sigma_c^2}{a\Gamma_3K_3T_{32}^2} \times$$

$$\times\left\{1 + \left[1 + \left(\frac{2C_3\tau\, T_{32}K_3}{S_3x_3\,\sigma_c\beta}\right)^2\right]^{1/2}\right\} \qquad (140)$$

where σ_c is the debonding criterion, T_{32} is defined by Equation (137), and β is defined by Equation (133).

The optimum blackbody temperature is given by Equation (23) or (24), depending on the value of b.

10.11 DEBONDING OF A METAL/BOND/SUBSTRUCTURE DUE TO MAXIMUM THERMOMECHANICAL TENSILE STRESS GENERATED IN THE METAL

The maximum peak tensile stress generated in the metal is given by Equation (79). Since tensile stress waves are assumed not to attenuate, the tensile stress in the bond is given by Equation (79) multiplied by the transmission coefficient, T_{12}, between the metal and the bond. Subscripts 1

and 2 refer to the metal and bond, respectively. T_{12} is defined by Equation (137). The fluence threshold ϕ_t is thus given by

$$\phi_t = \frac{96 C_{1^\tau} \sigma_c}{k \Gamma_1 T_{12}} \left[1 - \exp \left(- \frac{2 \rho_1 D_r C_{1^\tau}}{k \phi_t} \right) \right]^{-1} \tag{141}$$

This is a transcendental equation for ϕ_t which must be solved by successive approximation. However, the exponential term is insensitive to ϕ_t and the initial estimate of ϕ_t ignores it. The second approximation includes the numerical value of the exponential term which is evaluated using the initial estimate of ϕ_t. This process is repeated until ϕ_t converges, usually requiring only two successive approximations; i.e., an initial estimate and a second and final estimate.

The optimum blackbody temperature is obtained from Equation (80) or by reference to energy-deposition curves.

10.12 DEBONDING BY STRUCTURAL RESPONSE TO MAXIMUM BLOWOFF IMPULSE

Combining Equations (115) and (118) gives directly the minimum ϕ_t for causing debonding by structural response to maximum blowoff impulse:

$$\phi_t = \frac{2 \sigma_c E_t^{1/2}}{A \Delta \omega} \tag{142}$$

The optimum blackbody temperature is given by Equation (51) or (52), depending on the blowoff impulse model used.

10.13 SHELL BUCKLING OR RUPTURE BY STRUCTURAL RESPONSE TO MAXIMUM BLOWOFF IMPULSE

Combining Equations (107) and (118) gives directly ϕ_t for causing shell buckling or rupture due to structural response to maximum blowoff impulse:

$$\phi_t = \frac{h \Gamma_m E_t^{1/2} \sigma_e}{AC} \tag{143}$$

where the effective stress-to-failure is

$$\sigma_e = \left[2E \int_{\epsilon_{st}}^{\epsilon_c} \sigma(\epsilon) d\epsilon \right]^{1/2} \tag{144}$$

and is equal to $(\sigma_c - \sigma_{st})$ for a linear stress-strain relationship, where σ_{st} refers to the static stress.

The optimum blackbody temperature is given by Equation (51) or (52), depending on the blowoff model used.

10.14 SHELL BUCKLING OR RUPTURE BY STRUCTURAL RESPONSE TO MAXIMUM NONBLOWOFF IMPULSE

Combining Equations (107), (109), and (144) gives directly ϕ_t for causing shell buckling or rupture due to maximum nonblowoff impulse (i.e., no front-face mass removal occurs) in liquid propellant tankage:

$$\phi_t = 48 \left(\frac{h}{C_t}\right) F_m \sigma_e \left[\frac{\Gamma_t}{C_t} f + \frac{\Gamma_\ell}{C_\ell} (1 - f) \right]^{-1} \tag{145}$$

The optimum blackbody temperature is the temperature that maximizes the bracketed term, with the constraint that the surface dose is less than the mass removal dose criterion. There is no equation for this, but usually a good approximation (when $\Gamma_t/C_t \simeq \Gamma_\ell/C_\ell$ is simply to meet the surface dose constraint. For this, the blackbody temperature is given either by Equation (80) or Figures 2 through 7, depending on the atomic number of the tank material.

10.15 SIZING OF STRESS WAVE ATTENUATOR FOR MAXIMUM BLOWOFF IMPULSE

Combining Equations (105) and (118) gives directly the thickness of a porous stress wave attenuator material for maximum blowoff impulse:

$$h = 0.032A\phi \left[E_t \sigma_c \rho f_v (1 - f_v)/T_t \right]^{-1/2} \qquad (146)$$

where T_t is given by Equation (106). The optimum blackbody temperature is given by Equation (51) or (52), depending on the blowoff model used.

10.16 SUMMARY

The relationships for optimum spectra judged to be the most useful are summarized in Tables 4 and 5. It is convenient in generalizing the analysis of x-ray effects to categorize materials as either surface or subsurface. In this framework, Table 4 is for surface materials, and Table 5 is for subsurface (shielded) materials.

As applicable, equations are shown for determining fluence thresholds and for calculating the magnitude of the effect in question. For convenience, one blowoff model, MBBAY, has been used. The symbol Z in the equations refers in general to the effective atomic number Z_e. (See Section 2.5 for a discussion of situations involving $6 < Z_e < 12$.)

The equations, as shown in the tables and throughout the report, are all for normally incident radiation. For oblique incidence, the same relationships hold exactly (i.e., no analytical approximation is involved), except for appropriate scaling with the cosine of the incidence angle. Oblique incidence may be a consideration for a surface whose size is large compared to material thicknesses. The equations are modified for oblique incidence as follows.

It can be shown that for all dose relationships that involve a fixed affected thickness, oblique incidence is treated exactly by the relationships for normal incidence if the fluence is scaled as follows:

$$\phi_o = \phi_n \cos\Theta \qquad (147)$$

where Θ is the incidence angle as measured from the normal. That is, for normal incidence, $\Theta = 0$. The normally incident fluence in the equations is

TABLE 4

GENERALIZED DESIGN EQUATIONS FOR SURFACE MATERIALS

DESIGN EQUATIONS		OPTIMUM BLACKBODY EQUATIONS	REMARKS
THRESHOLD	EFFECT		
1. a Threshold for a Specified Peak Dose at Front Surface $\phi_t = \frac{D_c T^3}{3Z^3}$, $Z \leq 6$ $\phi_t = \frac{D_c T^2}{60Z}$, $Z \geq 12$	1. b Peak Dose at Front Surface for a Specified Fluence $D_o = \frac{3Z^3 \phi}{T^3}$, $Z \leq 6$ $D_o = \frac{60 Z \phi}{T^2}$, $Z \geq 12$	Optimum temperature is lowest of interest.	Peak dose is calculated for specific temperature. Peak surface dose in any surface material increases with decreasing temperature.
2. a Threshold for a Specified Amount of Front-Face Mass Removal $\phi_t = 4.2 D_r \rho X_r$	2. b Front-Face Mass Removal for a Specified Fluence $X_r = \frac{0.24 \phi}{\rho D_r}$	$T_o = 0.5 Z(\rho X_r)^{1/3}$, $Z \leq 6$ $T_o = 1.2 Z^{4/5}(\rho X_r)^{2/5}$, $Z \geq 12$	
3. a Threshold for a Specified Peak Equilibrium Temperature Rise See Remarks.	3. b Peak Equilibrium Temperature Rise for a Specified Fluence $\Delta T = 0.2\left(\frac{\phi}{\rho X c_p}\right) + 0.43\left(\frac{D_r}{c_p}\right)$, $0.37 \leq \frac{\rho X D_r}{\phi} < 1$. $\Delta T = \left(\frac{\phi}{\rho X c_p}\right)\left(1 - e^{-\frac{\rho X D_r}{\phi}}\right)$, $\frac{\rho X D_r}{\phi} \geq 1$.	$T_o = 0.5 Z(\rho X)^{1/3}$, $Z \leq 6$ $T_o = 1.2 Z^{4/5}(\rho X)^{2/5}$, $Z \geq 12$	Equilibrium thermal temperature is the average temperature through the material thickness. Equation is transcendental in ϕ, and ΔT vs ϕ must be plotted to find $\phi = \phi_t$. See Figure 4-2.
4. a Threshold for Back-Face Spall Due to Blowoff Impulse $\phi_t = \frac{0.31 S X \sigma_s^2 E_m^{1/2}}{C K T_r^2}\left\{1 + \left[1 + \left(\frac{2C\tau K T_r}{S X \sigma_s}\right)^2\right]^{1/2}\right\}$	4. b Peak Back-Face Reflected Stress Due to Blowoff Impulse for a Specified Fluence $\sigma_p = \frac{1.6\phi T_r}{\tau E_m^{1/2}}\left(1 + \frac{1.6 S X \phi}{K C \tau^2 E_m^{1/2}}\right)^{-1/2}$	$T_o = 0.24 Z(\frac{\phi}{E_m})^{1/3}$, $Z \leq 6$ $T_o = 0.52 Z^{4/5}(\frac{\phi}{E_m})^{2/5}$, $Z \leq 12$	Accounts for a bonded subsurface material via a stress wave reflection coefficient T_r. Negative T_r indicates tensile stress.
5. a Threshold for Shell Buckling or Rupture by Structural Response to Blowoff Impulse $\phi_t = 0.63 \frac{X F_m E_m^{1/2}}{C} \sigma_e$	5. b Deflection is not a good general indicator of damage.	Same as (4) above.	Applicable for a single shell or multi-shell structure. Shells must be contiguous but not necessarily bonded. For a linear stress-strain relationship, $\sigma_e = \sigma_c - \sigma_{st}$, where σ_{st} is the static stress.
6. a Threshold for Shell Buckling or Rupture by Structural Response to Non-Blowoff Impulse $\phi_t = 48 \frac{X}{C_t} F_m \sigma_e \left[\frac{\Gamma_t}{C_t} f + \frac{\Gamma_\ell}{C_\ell}(1-f)\right]^{-1}$	6. b Same as (5) above.	See Section 10.14.	Applies to liquid propellant tanks only. Maximum non-blowoff impulse implies no front-face mass removal. For a linear stress strain relationship, $\sigma_e = \sigma_c - \sigma_{st}$, where σ_{st} is the static stress.

TABLE 5

GENERALIZED DESIGN EQUATIONS FOR SUBSURFACE MATERIALS

DESIGN EQUATION		OPTIMUM BLACKBODY EQUATIONS	REMARKS
THRESHOLD	EFFECT		
1. a Threshold for a Specified Dose* $\phi_t = \frac{D_c(\Sigma_s)^b}{a}\left(\frac{Z_{es}^n}{Z_{ca}^n}\right)$	1. b Peak Dose for a Specified Fluence* $D = a\phi(\Sigma_s)^{-b}\left(\frac{Z_{ca}^n}{Z_{es}^n}\right)$	$T_0 = 0.5\,Z(\Sigma_s)^{b/3}$, $Z \leq 6$ $T_0 = 1.2\,Z^{4/5}(\frac{2b}{5})^{\frac{2b}{5}}$, $Z \geq 12$	For any subsurface material shielded by any number of other materials.
2. a Threshold for Back-Face Spall of a Bonded Subsurface Material Due to Blowoff Impulse in the Surface Material $\phi_t = \frac{0.31\,\sigma_s^2 E_m^{1/2}\Sigma_i}{C T_t^2 T_r^2}\left\{1 + \left[1 + \left(\frac{2C\tau T_t T_r}{\sigma_s \Sigma_i}\right)^2\right]^{1/2}\right\}$	2. b Peak Back-Face Reflected Stress in a Bonded Subsurface Material Due to Blowoff Impulse in the Surface Material for a Specified Fluence. $\sigma_p = \frac{1.6\phi T_t T_r}{\tau E_m^{1/2}}\left(1 + \frac{1.6\phi\Sigma_i}{C\tau^2 E_m^{1/2}}\right)^{-1/2}$	$T_0 = 0.24\,Z(\frac{\phi}{E_m})^{1/3}$, $Z \leq 6$ $T_0 = 0.52\,Z^{4/5}(\frac{\phi}{E_m})^{2/5}$, $Z \geq 12$	Back-face need not be a free surface and is accounted for by the stress reflection coefficient, T_r. Negative T_r indicates tensile stress.
3. a Threshold for a Specified Peak Compressive Stress in a Bonded Subsurface Material Due to Blowoff Impulse in the Surface Material Same as 2. a with $T_r = 1$.	3. b Peak Compressive Stress in a Bonded Subsurface Material Due to Blowoff Impulse in the Surface Material for a Specified Fluence Same as 2. b with $T_r = 1$.	Same (2) above.	
4. a Threshold for a Specified Peak Thermomechanical Compressive Stress in a Non-contiguous Single Subsurface Material, or any Part of a Laminated Subsurface Structure* $\phi_t = \frac{96\,b\,C\tau\,\sigma_c\,\Sigma_s^{b-1}}{a\Gamma T_t A}\left[1 + \frac{a\Gamma A^2\Sigma_i}{96b\,C^2\tau^2\Sigma_s^{b-1}}\right]^{1/2}$ $A = 1 - \exp\left[-\frac{2b\rho C\tau}{\Sigma_s}\left(\frac{Z_{ca}^n}{Z_{es}^n}\right)\right]$	4. b Peak Thermomechanical Compressive Stress in a Non-Contiguous Single Subsurface Material, or any Part of a Laminated, Subsurface Structure for a Specified Fluence* $\sigma_p = \frac{a\Gamma T_t \phi A}{96bC\tau\,\Sigma_s^{b-1}}\left[1 + \frac{a\Gamma A^2\Sigma_i}{96\,bC^2\tau^2\Sigma_s^{b-1}}\right]^{-1/2}$	Same as (1) above.	Material properties are for the subsurface material in which the stress is generated, which is the first non-contiguous shielded materials.
5. a Threshold for Debonding of a Composite/Bond/Metal Structure Due to Blowoff Impulse in the Surface Composite Material $\phi_t = \frac{0.31\,\sigma_d^2 E_m^{1/2}\Sigma_i}{CT_t^2}\left\{1 + \left[1 + \left(\frac{2C\tau T_t}{\sigma_d \Sigma_i}\right)^2\right]^{1/2}\right\}$ $T_t = T_{12} T_{23} T_{32}$	5. b Peak Tensile Stress in Bond of a Composite/Bond/Metal Structure Due to Blowoff Impulse in the Surface Composite Material for a Specified Fluence $\sigma_p = \frac{1.6\phi T_t}{\tau E_m^{1/2}}\left(1 + \frac{1.6\phi\Sigma_i}{C\tau^2 E_m^{1/2}}\right)^{-1/2}$	Same as (2) above.	Compressive stress propagates into metal, reflects as tensile and returns to bond. Subscripts 1, 2, and 3 refer to composite, bond, and metal substructure, respectively.
6. a Threshold for Debonding of a Composite/Bond/Metal Structure due to Thermomechanical Stress Generated in the Metal Substructure* $\phi_t = \frac{48bS_3X_3(\rho_1X_1 + \rho_2X_2)^{b-1}\sigma_d^2}{a\Gamma_3 K_3 T_{32}^2}\left\{1 + \left[1 + \left(\frac{2C_3\tau T_{32}K_3}{S_3X_3\sigma_d A}\right)^2\right]^{1/2}\right\}$ $A = 1 - \exp\left[-\frac{2b\rho_3 C_3\tau}{\rho_1X_1 + \rho_2X_2}\left(\frac{Z_{ca}^n}{Z_{es}^n}\right)\right]$	6. b Peak Tensile Stress in Bond of a Composite/Bond/Metal Structure Due to Thermomechanical Stress Generated in the Metal Substructure for a Specified Fluence* $\sigma_p = \frac{a\Gamma_3 T_{32} A\phi}{96b\,C_3\tau(\rho_1X_1 + \rho_2X_2)^{b-1}}\left[1 + \frac{a\Gamma_3 S_3 X_3 A^2\phi}{96b\,K_3 C_3^2\tau^2(\rho_1X_1 + \rho_2X_2)^{b-1}}\right]^{-1/2}$	Same as (1) above with $\Sigma_s = \rho_1X_1 + \rho_2X_2$	Subscripts 1, 2, and 3 refer to composite, bond, and metal substructure, respectively. Shielding materials are the composite and bond.
7. a Threshold for Debonding of a Metal/Bond/Substructure Due to Thermomechanical Tensile Stress Generated in the Surface Metal $\phi_t = \frac{96C_1\tau\sigma_d}{k_1\Gamma_1 T_{12}}\left[1 - \exp\left(-\frac{2\rho_1 D_1 C_1\tau}{k_1\phi_t}\right)\right]^{-1}$	7. b Peak Tensile Stress in Bond of a Metal/Bond/Substructure Due to Thermomechanical Tensile Stress Generated in the Surface Metal for a Specified Fluence $\sigma_p = \frac{E_1\Gamma_1 T_{12}\phi}{96C_1\tau}\left[1 - \exp\left(-\frac{2\rho_1 D_1 C_1\tau}{k_1\phi}\right)\right]$	See Section 6.2.3.	Subscripts 1 and 2 refer to metal and bond, respectively. This equation must be evaluated by successive approximation.
8. a Threshold for Debonding by Structural Response to Blowoff Impulse $\phi_t = \frac{1.25\,\sigma_d E_m^{1/2}}{\Delta\omega}$	8. b Peak Tensile Stress in Bond of a Composite Structure Due to Structural Response to Blowoff Impulse for a Specified Fluence $\sigma_p = 0.8\phi\,\Delta\omega\,E_m^{-1/2}$	Same as (2) above.	Not likely to be a critical failure mode.

*See Table 2-1 for values of a, b, and n

ϕ_n, and ϕ_o is the corresponding obliquely incident fluence. In other words, for a specified ϕ (the Effect column of Tables 4 and 5), the quantity to be substituted for ϕ in the equations is $\phi \cos \theta$. Conversely, for a calculated threshold ϕ_t (the Threshold column of Tables 4 and 5), the normally incident threshold for oblique incidence is $\phi_t/\cos \theta$. For T_o, substitute $\rho x/\cos \theta$ for ρx and $\Sigma_s/\cos \theta$ for Σ_s. In considering oblique vs. normal incidence, as a general rule the effects for oblique incidence are less, thresholds are greater, and optimum temperatures for other than blowoff impulse are greater. Quantities that do not change with incidence angle are: (1) the surface dose for a surface material because thickness is not involved, and (2) the optimum temperature for blowoff impulse because the energy/mass ratio must remain the same. The fact that T_o for maximum blowoff impulse does not change with θ is implied by Figure 12, which indicates that for a fixed η, ℓ is proportional to ϕ regardless of θ. By the same token, for a specific spectrum (i.e., a fixed ℓ), η varies with cos θ according to how ϕ varies with cos θ.